Design and Validation of a Supercritical Water Gasification Reactor with *In Situ* Raman Spectroscopy for the Determination of Chemical Kinetic Rates

David Gorman

A thesis
submitted in partial fulfillment of the
requirements for the degree of

Master of Science in Mechanical Engineering

University of Washington
2018

Thesis Committee:
Igor V. Novosselov, Chair
John C. Kramlich
Per Reinhall

Program Authorized to Offer Degree:
Department of Mechanical Engineering

University of Washington

Abstract

Design of a Supercritical Water Gasification Reactor with *In-Situ* Raman Spectroscopy for the Determination of Chemical Kinetic Rates

David Gorman

Chair of the Supervisory Committee:
Prof. Igor V. Novosselov
Department of Mechanical Engineering

Supercritical water technology has the potential to enable the safe and complete destruction of hazardous chemical compounds, including chemical waste and chemical warfare agents. While the underlying technology shows promise, quantitative determination of chemical kinetic rates under these conditions are needed to facilitate the design of full scale technology. Collecting these needed data requires a versatile reactor capable of determining chemical decomposition rates. Critical parameters include temperature, residence time, and catalytic wall effects. The literature shows significant differences in the published chemical kinetic rates, which is at least partially attributed to variations in reactor design. To determine best practices, existing reactor designs, components, and technologies, as well as some promising new technologies, are reviewed. From this overview, a reactor specialized for the gasification of organic compounds was designed featuring *in situ* Raman monitoring of the effluent stream. In addition to the design of the reactor, some basic processing techniques for Raman baseline signal subtraction are discussed, along with preliminary results for organic compounds decomposition. With the reactor completed, the rapid determination of chemical kinetic rates in supercritical water becomes possible for a wide range of reagents and operating conditions.

TABLE OF CONTENTS

TABLE OF FIGURES

ACKNOWLEDGMENTS

The work conducted during my time at the University of Washington was made possible by Grant HDTRA1-17-1-0001 from the Defense Threats Reduction Agency of the Department of Defense. The resources available at the University of Washington as well as the expertise of the Novosselov Research Group made this work possible.

I would like to thank my advisor, Dr. Igor Novosselov, for his mentorship and trust in working on a new and exciting project. I am deeply grateful for the opportunities I was given while working for Dr. Novosselov. I would also like to thank my other committee members, Professor John Kramlich and Professor Per Reinhall. Being able to brainstorm and troubleshoot with you in meetings proved invaluable. In addition, I extend my gratitude to Giora Proskurowski at MarqMetrix for his continued support with adapting and troubleshooting the Raman optical cell for our design.

In addition, I would like to thank Brian Pinkard, Kartik Tiwari, Justin Davis, Elizabeth Rasmussen, and Vedant Maheshwari for their help as members of the supercritical fluids team. I never could have built this system without their help and varied expertise. The members of the Novosselov Research Group have my thanks for providing good conversation, help understanding lab and university procedure, and on some occasions, taste testing my home-brew.

Finally, I would like to thank my friends and family who supported me through my time at the University of Washington, especially my father for giving me a place to stay amid rising housing costs and my mother for convincing me that I needed a cat.

CHAPTER 1: INTRODUCTION

Supercritical fluids possess unique physiochemical properties that enable their use as media for chemical processes, such as waste treatment, organic compounds gasification, material synthesis, etc. At temperatures and pressure above the critical point, fluids properties can be varied continuously from liquid-like to gas-like without inducing a phase change. Operating in this region provides a highly-tunable reaction medium that can be optimized for various processes. In order to transition the supercritical fluid technology to industrial scale applications, the underlying chemical processes have to be studied and optimized in the laboratory scale system. These optimization study parameters may include operational conditions such as pressure and temperature, as well the guidance for system design such as heating strategies, reactor surface to volume ratio, control and process monitoring, catalyst introduction, etc.

Supercritical water is one of the earliest supercritical fluids investigated for potential chemical processing due to a unique set of thermophysical properties that make it a particularly attractive solvent. Unlike supercritical CO_2, which reaches its critical point at a relatively low 31.1°C, the high temperature of supercritical water is well-suited for chemical reactions related to decomposition of organic compounds. The dependence of the dielectric constant on temperature and pressure near the critical point also allows water to be tuned to dissolve either polar or non-polar molecules. The transition from a polar to non-polar solvent derives from the decreases in density, dielectric constant, and quantity of hydrogen bonds [1]. Figure 1 shows the density and dielectric constant isobars as a function of temperature near the critical region. The plot is computed using NIST REFPROP software [2, 3] which allows water properties to be estimated over large temperature and pressure regions. The primary advantages of supercritical water derive from the fact that it behaves as a non-toxic organic solvent, allows chemistry to take place in a

single fluid phase, and possesses highly tunable thermophysical properties relative to room temperature water [4].

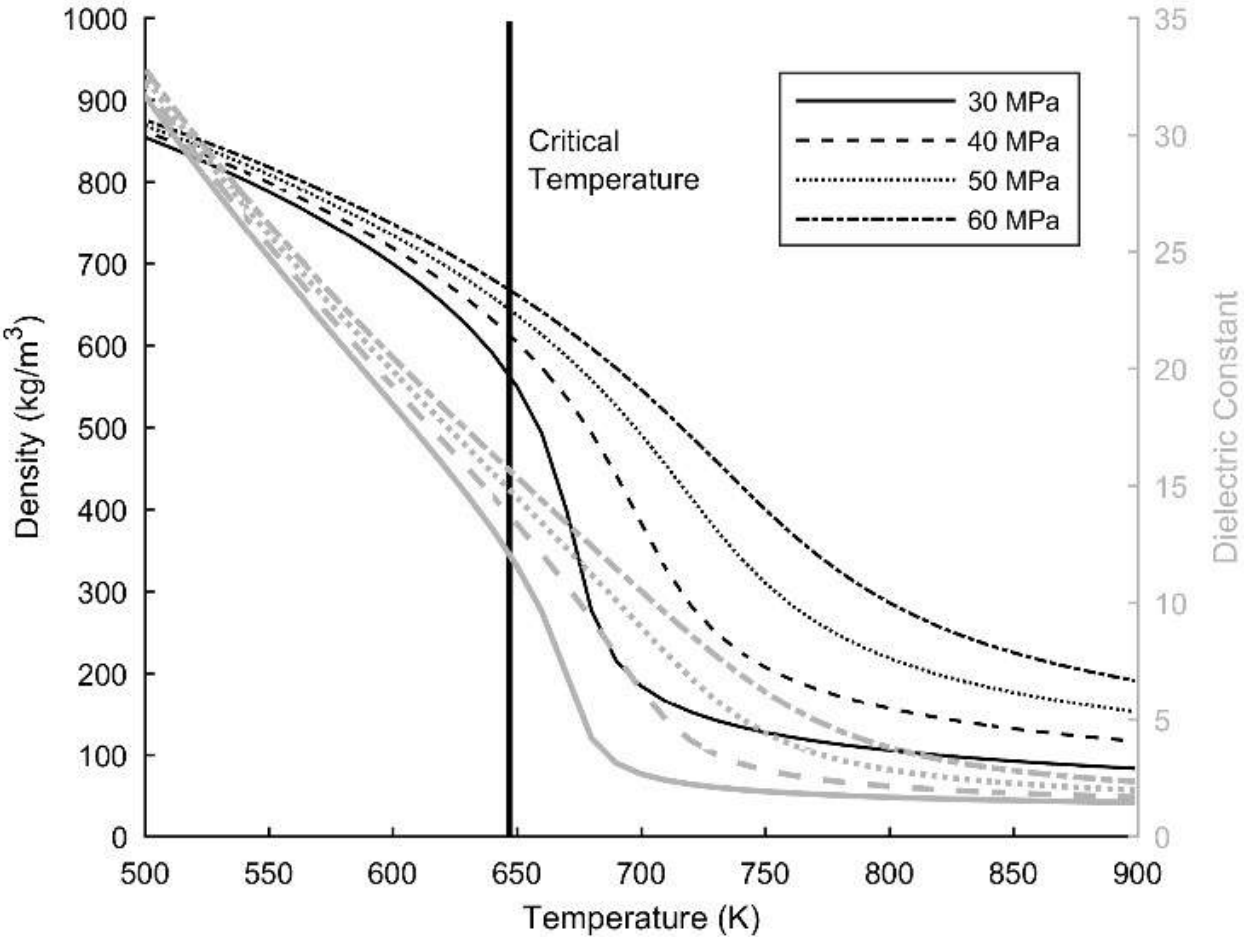

Figure 1: Density and dielectric constant isobars across the critical point of water, generated using data from the NIST REFPROP software [2, 3]. By varying both pressure and temperature, a wide variety of properties can be chosen.

Since the early 1980s, researchers have studied chemical reactions in supercritical water. Laboratory-scale batch and continuous reactors have been used to determine chemical kinetic rates of multiple model compounds, including various biomass and organic feedstocks, and have led to the development of pilot and industrial scale reactors [5]. Supercritical water reactors (SCWR)

include supercritical water oxidation (SCWO) and supercritical water gasification (SCWG) reactors [6, 7].

Supercritical water oxidation technology is primarily used in the destruction of toxic waste. Under supercritical conditions, both organic compounds and oxygen become fully miscible in water, allowing oxidation to occur in a single fluid phase. Oxidation in supercritical water often compares favorably to wet air oxidation and incineration [8]. Most organic compounds can achieve complete oxidation in less than one minute with optimized temperature and pressure. Processing wastewater and sludge has been the most common application for SCWO technology [9].

Supercritical water gasification produces light gases, such as hydrogen, carbon monoxide, and methane from organic feedstocks such as biomass and organic process waste. These gases can then be stored for use as fuel. Most research in supercritical water gasification has considered processing biomass and biomass surrogates [4, 5, 10], and some research into the gasification of sewage sludge has been conducted [11-13]. Lignin and cellulose both gasify rapidly in supercritical water, and the technology is considered carbon neutral [4]. A schematic of a typical SCWG system is shown in Figure 2. While laboratory systems can be fairly flexible in their design and operation, the design of industrial-scale reactors is more complicated; it requires insight into kinetic rates for optimization of reactor operation and geometry, material and hardware selection, process monitoring and control, catalyst selection, and process economics. The laboratory reactor studies can address some of these considerations.

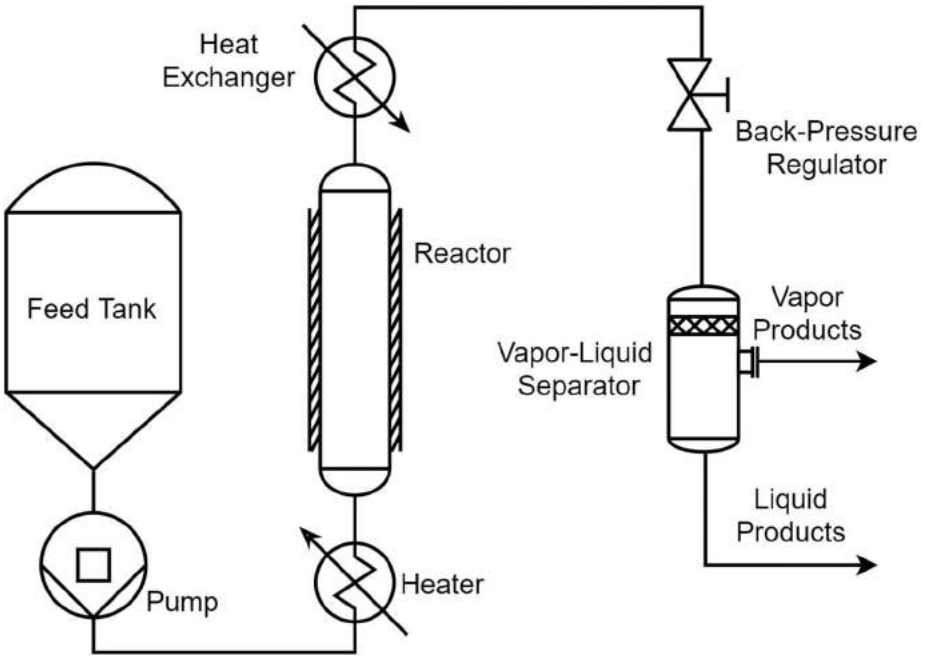

Figure 2: General schematic of a typical SCWG reactor system with premixed water and reagent. The reagent can also be injected after preheating the water using a mixing section

In the application of SCWO to organic waste disposal, the chemicals entering the system often pose a health risk. The concentration of hazardous chemicals in the effluent must be reduced to acceptable levels before exiting the reactor. A well-designed SCWO system should reduce concentrations of hazardous chemicals to acceptable levels as quickly as possible and without wasting excess oxidant or energy. For SCWG, the yield of product gases depends on reaction pathways and their chemical rates. Maximizing hydrogen production is a common goal for biomass gasification; insight into the reaction pathways and their respective rates allows for the optimization of product gas composition without unnecessary energy expenditures [4, 14, 15]. A recent review of gasification rates and pathways in supercritical water has shown that product yields and intermediate species are highly dependent upon the reaction temperature, residence time, and choice of feedstock [16].

Two types of reactors are employed in studies of chemical kinetic rates: batch reactors and continuous flow reactors. In batch reactors, a known quantity of water and reagents are pressurized, heated, and held at the reaction conditions for a set amount of time. In a continuous flow reactor, water and reagents are combined in a continuous process where residence time is determined by flow rates, reactor size, and operating parameters. Continuous and batch reactors face a different set of design challenges, although the continuous process promises higher-throughput and improved economics for a larger scale system. The chemical rates and reaction pathways may be significantly different between these two types of reactors due to the catalytic wall effect [17]; the reactor surface-to-volume ratio, reagent mixing schemes, or other differences [16] can play a significant role in reaction kinetics. Here, we aim to provide an overview of the designs of the continuous supercritical gasification process; the design of batch reactors is not considered in this review.

Continuous SCWG and SCWO reactors face similar challenges regardless of design intent; these include (i) corrosion of reactor walls and components, (ii) achieving and controlling high pressure and temperature within the reactor, and (iii) acquiring time-resolved chemical species information for process quality control or reaction rate analysis. The design of oxidation systems is further complicated by the introduction of oxidant into the reactor as a liquid feed (often as H_2O_2) or compressed gas (oxygen or air), which may lead to safety concerns. In the design of a supercritical water reactor, choices about each subsystem must be tailored to the desired application. Systems for pressurization, heating, mixing, reaction, cooling, and sample analysis must be considered, as well as a choice of material and control strategies.

This thesis provides an overview of the various design choices and operational parameters that affect the performance of continuous lab-scale SCWRs. Two early prominent SCWR systems are

reviewed in detail, and other reported reactor designs are summarized. Common challenges and the advantages of various solutions presented in the literature are analyzed. Reactor components for the UW SCWR are detailed with justification as to their selection and issues encountered along with their solutions are discussed.

CHAPTER 2: SYSTEM REVIEW

Early Reactor Designs

The designs of the reactor from the lab of Jefferson Tester at MIT and the Supercritical Fluids Reactor (SFR) at Sandia National Laboratories provide two different examples of early SCWR systems. The choice of heating, pressurization, sampling, and control systems differs between these reactors, but together they have provided a framework for the design of other laboratory supercritical reactor systems. The MIT system laid a foundation for supercritical water research and is widely cited in scientific literature, while the Sandia reactor provides the most detailed description of all reactor ancillary components. The Sandia reactor was designed to operate over a large operational space with a high degree of flexibility to maximize the types of studies that could be performed. Table 1 summarizes the operating parameters and the materials used in each reactor system.

Table 1: Operating parameters and material used in the Sandia SFR and MIT reactor. The SFR was built over a decade after the MIT reactor and was designed to perform a wider variety of experiments over a larger range of conditions.

Reactor	Temperature Range (°C)	Operating Pressure (MPa)	Residence Time (s)	Water Flow Rate (g/s)	Material
MIT Reactor	400-540	24.6	6-14	0.17	Inconel 625 & Hastelloy C-276
Sandia SFR	375-650	22-43	0.09-250	0.17-2.0	Inconel 625

The MIT reactor is one of the earliest academic SCWRs. It was built in the early 1980s and was used to determine oxidative kinetic rates of carbon monoxide, ammonia, and ethanol [18, 19], as well as methane [20]. Many other experiments were conducted in later years using the same reactor design, although subsequent studies modified the original reactor design [21]. The Ph.D. thesis of Helling describes the overall design and components used in the construction of the reactor [22]. Figure 3 shows a simplified schematic of the reactor and its system components.

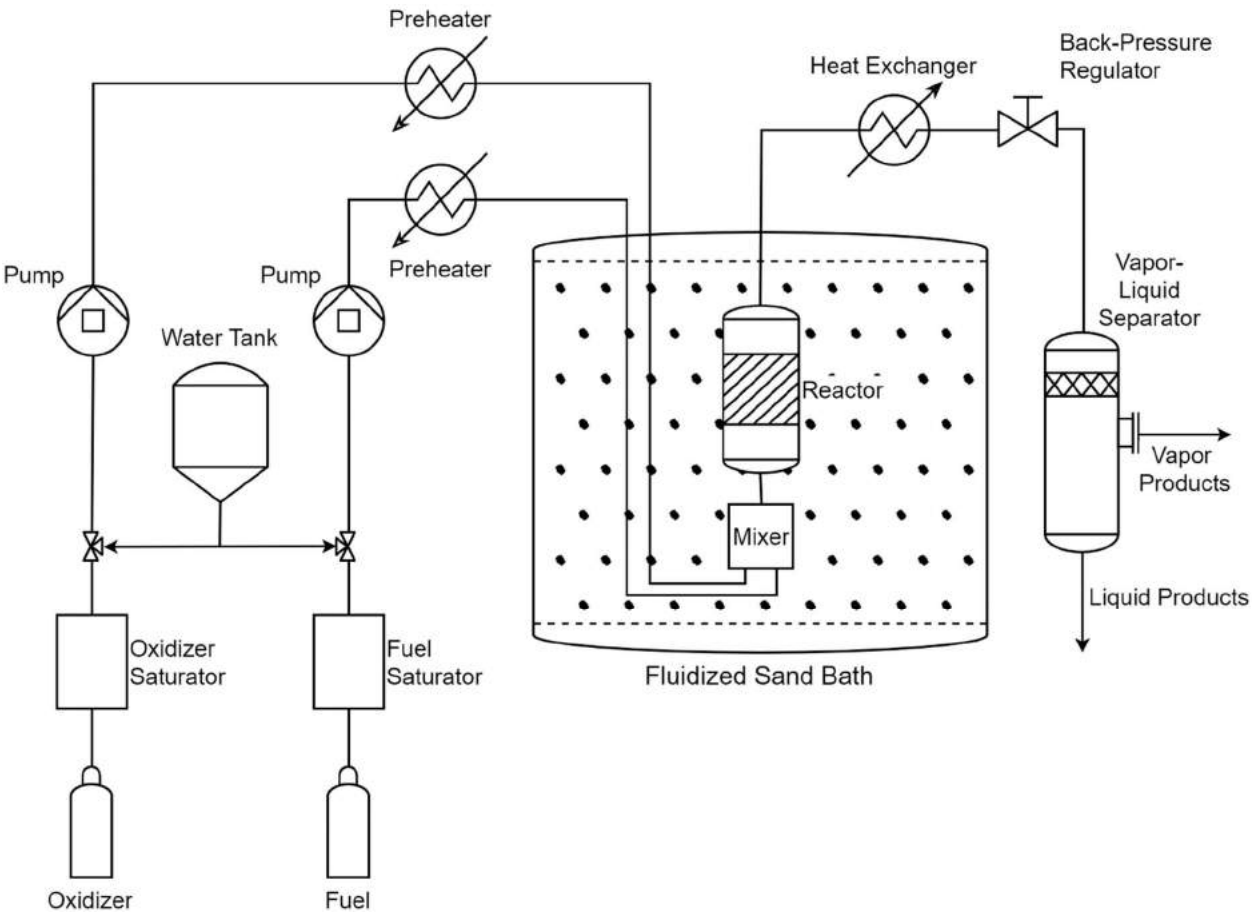

Figure 3: Simplified schematic of the MIT reactor built in the early 1980s. The design would later change to include new heaters and a superior mixing section.

The tubing and fittings of the reactor system consisted of Hastelloy C-276 and Inconel 625. These two nickel-based alloys have excellent corrosion resistance and retain strength at elevated temperatures. The reactor section was designed to be isothermal and well-mixed, and the reactor was assumed to operate in a plug-flow regime to simplify the kinetic analysis. The reagents and primary flow of supercritical water were heated separately and mixed at the inlet of the reactor section. Electrical heaters were used to bring the separate streams to the reaction temperature before mixing, while a fluidized sand bath maintained an isothermal condition for the entire length of the reactor section. At the reactor exit, a heat exchanger rapidly quenched the reaction before

throttling the stream to low pressures through a back-pressure regulator. Reducing the pressure of the effluent stream caused a partial phase change that separated the effluent into a liquid and gas. Both gas and liquid samples were analyzed ex-situ using a variety of methods depending on the experiment conducted (including gas chromatography, total organic carbon analysis, pH measurements, and others). Thermocouples and pressure sensors were used to monitor process parameters at various points in the reactor system. Over the course of the experiments performed by Helling, the reactor temperature ranged from 400 to 540°C at a constant pressure of 24.6 MPa. The mass flow rate in the reactor was kept to a constant 10 g/min, with Reynold's numbers around 3100 and residence times between 6 and 14 seconds [22].

Sandia built the SFR in the 1990s and designed it to conduct a wide variety of SCWG and SCWO experiments. Extensive documentation exists in a report [23], providing insight into the design philosophy and operating details of the SFR. The reactor includes several unique components and subsystems not present in other supercritical fluids reactors of the time. Specifically, real-time monitoring was implemented using an optical cell for *in situ* Raman spectroscopy, and a modular reactor design allowed residence times to vary dramatically. A simplified schematic of the SFR is presented in Figure 4.

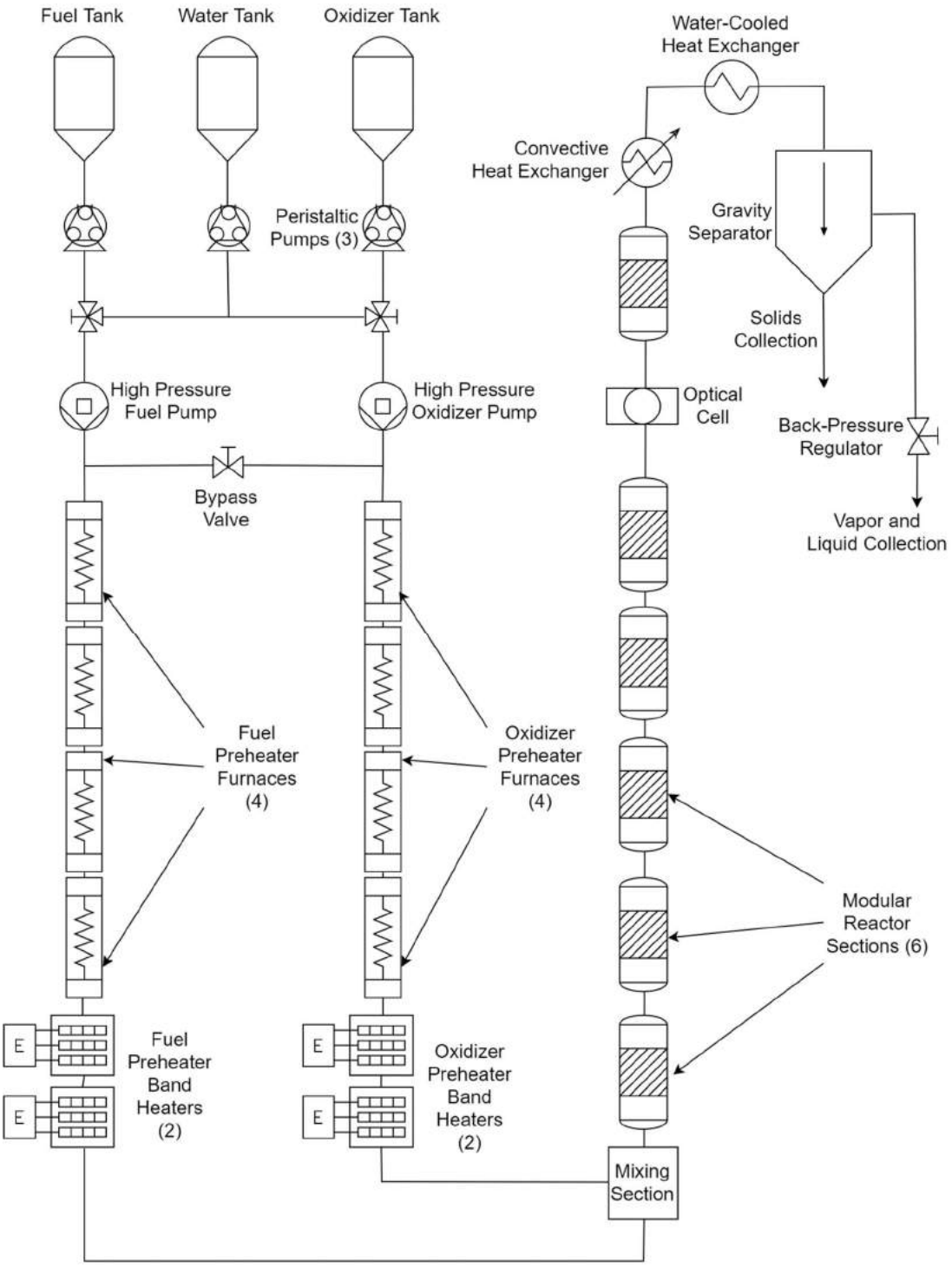

Figure 4: Simplified schematic of the SFR developed at the Sandia National Laboratories.

The SFR consisted of several main subsystems: pressurization, feed injection, preheating, reactor, cooling, and the separation of products. These subsystems exist in all SCWRs, although the design, component selection, and complexity of each subsystem vary. Similar to the MIT reactor, all high-temperature components on the SFR were fabricated from the nickel-based alloy Inconel 625. To independently control flow rate and pressure inside the reactor, high pressure, positive displacement piston pumps provided a constant flow rate, while back pressure regulators controlled the pressure. Water and reagent feeds could be mixed before heating or heated separately and then introduced into a mixing section. Each preheat section contained six separate stages. The first four stages consisted of radiative furnaces, while the final two stages used resistive cable heaters.

The reactor section contained six identical segments that could be assembled in series. Each section was insulated and contained a resistive cable heater and a convection cooler to precisely control temperature at every location within the reactor. Installing both heating and cooling elements allowed the reactor to operate isothermally during both exothermic oxidation reactions and endothermic gasification reactions. Each reactor segment measured 0.61 meters in length with an external diameter of 14.3 mm and an internal diameter of 4.8 mm. The optical cell could be placed between any of the reactor segments and was heated using two resistive band heaters. Insulation covered both the band heaters and the optical cell.

The SFR operated at temperatures between 375°C and 650°C with pressures between 22.4 MPa and 43.4 MPa. By using a large, modular reactor the residence time could be varied from 0.09 to 250 seconds. The mass flow rate of water in the system ranged from 0.17 to 2.0 g/s. Depending on its placement within the reactor section, the optical cell could take measurements for residence times between 0.09 and 81.2 seconds. For residence times outside the optical cell's range, sample

analysis methods such as gas chromatography and total organic carbon analysis were used to determine species concentration.

Design Considerations

While the MIT and Sandia reactors provide good insight into the design and fabrication of SCWR systems, other reported continuous SCWR reactors show that some changes in the design can benefit more specialized applications. Reactor costs and research focus determine the reactor design complexity and choice of components. Corrosion mitigation, pressurization, heating, cooling, data acquisition, and mixing have several approaches, while other systems have a standard solution applied in virtually all SCWR systems.

After the flow leaves the reactor section, all SCWR systems have essentially the same systems: a heat exchanger to cool the flow, and a pressure regulator to depressurize the system. The flow is often separated into gas and liquid streams after this point, but this depends on the experiments being conducted. The general design criteria for selecting less universal subsystems in the published literature are discussed and tabulated below.

Corrosion Mitigation

Corrosion control methods in supercritical water have been extensively studied since the middle of the 20th century [24, 25]. Multiple reviews include an application for heat transfer and chemical reactors [9, 26, 27]. In the heat transfer applications, one does not need to account for the presence of species other than water in the heat transfer media. The high pressure and temperature and the corrosive environment associated with the presence of species of other than water are linked, presenting a significant challenge that has been an area of active research [28, 29]. Four primary methods for minimizing corrosion have been described in a recent review [30]. These approaches

include (i) preventing corrosive species from interacting with the reactor surface, (ii) forming a corrosion-resistant barrier on the interior surfaces of the reactor, (iii) taking steps to minimize corrosion inside the reactor, and (iv) tuning the reactor operating conditions to avoid severe corrosion scenarios. These approaches are often compatible with one another, allowing multiple strategies to coexist within the same system. While useful in large-scale or commercial SCWR systems, some of these corrosion mitigation techniques are not appropriate for laboratory studies of chemical kinetic rates. For example, in a reactor designed for the study of kinetic decomposition rates, preventing contact with reactor walls would introduce a concentration gradient within the flow. A plug flow regime inside the reactor eliminates the gradient and simplifies the determination of chemical kinetic rates, but this increases contact between the walls and corrosive species in the supercritical fluid.

Certain nickel-based alloys have been found to resist corrosion in the presence of salt precipitates that are likely to form in most practical applications of real-world feedstock and in the neutralization of chemical waste. The majority of continuous SCWRs have been constructed from Hastelloy C-276 or Inconel 625 due to the combination of excellent corrosion resistance and high strength at elevated temperatures. Tang et al. show that these two alloys tend to gain mass in the presence of corrosive species, while stainless steels tend to lose mass [31]. A buildup of deposits can be cleaned periodically, but lost mass in stainless steel reactors would eventually lead to the system falling out of safety standards and needing to be replaced. Nickel has a catalytic effect on many reactions in supercritical water, and this effect tends to decrease as the reactor walls undergo aging in supercritical water [5, 10]. This is assumed to be due to carbon building up on reactor walls and preventing access to the catalytic nickel surfaces. Titanium and platinum liners were successfully used in the operation of the SCWO reactors designed for destruction of chemical

warfare agents [32, 33]. Titanium alloys, while rarely used in laboratory-scale reactors, may potentially offer better corrosion resistance than nickel-based alloys for gasification in the presence of high heteroatom concentrations [31].

Pressurization

For all supercritical water reactors, pressurizing the reactor is one of the core subsystems. Any pressurization method should meet the following criteria: (i) capable of reaching pressures above the critical point, (ii) a constant, user-specified flow rate, (iii) low variation and pulsation in the flow rate during operation, and (iv) a range of flow rates to enable a variety of residence times without requiring physical changes to the reactor.

Among the reported laboratory systems, the most common way to achieve an independent flow rate and pressure control is to use a constant flow rate pump and a back-pressure regulator (BPR). For a consistent flow rate at high pressures, positive displacement pumps are a good choice at the laboratory scale. Though several types of pumps are available (such as a piston, peristaltic, syringe, and diaphragm pumps), dual-piston pumps are the most common in reviewed systems. These pumps use two piston heads to deliver constant flow with minimal fluctuation. However, these do not typically control delivery pressure; pressure control is achieved by using a BPR. Due to their compact size, integrated controls, and excellent reliability, high-performance liquid chromatography (HPLC) pumps are often used. These pumps typically operate with high flow-rate precision over a large range of flow rates, which has the added benefit of allowing residence times within the reactor to vary without making any adjustments to the physical reactor length or sampling location. Due to their low flow rates, HPLC pumps are not used in larger reactors, such as the Scaled-up Reactor System (SRS) [34], the ICMCB scale pilot plant [35], or the SCWO pilot

plant at the University of Cádiz [36]. A summary of some of the most common pump types and the systems in which they appear is presented in Table 2.

Table 2: Pump types used by reactors and the documenting article

HPLC or Piston	Diaphragm or Plunger	Syringe, Peristaltic, or Other
Zhang et al. [14]	Kruse [5]	Helling & Tester [18]
DiNaro et al. [21]	Elliot et al. [34]	Lester et al. [37]
Lester et al. [37]	Cansell et al. [35]	Caputo et al. [38]
Caputo et al. [38]	Benjumea et al. [36]	Nanda et al. [43]
Matsumura et al. [39]	Molino et al. [44]	Molino et al. [44]
González et al. [40]	Krammer et al. [50]	Anitescu et al. [45]
Steeper et al. [41]	Ondze et al. [51]	Thornton & Savage [52]
Ramayya et al. [42]		
Nanda et al. [43]		
Molino et al. [44]		
Anitescu et al. [45]		
Akizuki et al. [46]		
Sasaki et al. [47]		
Middelkoop et al. [48]		
Castello et al. [49]		

Heating

To reach supercritical condition, a large amount of heat must be supplied to the working fluid. For example, at 25 MPa, increasing the temperature from 20°C to 400°C requires an input of 2482.5 kJ/kg [2, 3]. This can be accomplished in different ways depending on researcher preferences and design goals. A review of laboratory system designs shows that there are three common strategies used in SCWR systems: immersive baths, resistive contact heaters, and electric furnaces. For example, the SFR used a combination of resistive band heaters and electric furnaces to provide heat into the system [23], while the MIT reactor used electric heaters coupled with a fluidized sand bath to ensure isothermal conditions [22].

Supercritical fluids have been shown to exhibit two irregular types of heat transfer: enhanced heat transfer (HTE) and deteriorated heat transfer (HTD) [53]. Near the critical point, HTE occurs due to the rapid change in properties, acting similar to boiling at lower pressures to keep walls cool at high heat fluxes. Away from the critical point, HTD can cause wall temperatures to spike well above the fluid temperature, potentially damaging the reactor walls. This poor heat transfer region must be considered for a robust and effective supercritical heating system. HTD can occur in one of two regions: at low mass fluxes in upward flows and systems with a combination of high mass flux and high heat flux. Smaller laboratory scale reactors operating at lower flow rates may suffer from HTD; the reduced heat-transfer coefficient at low mass fluxes appears to arise due to buoyancy effects in the heating section [53].

Electric furnaces typically come with high power ratings and built-in controls, making them a convenient and simple heating solution. These furnaces often contain multiple, independent

heating zones so that the temperature can be finely controlled over the length of the furnace. These heaters also come fully insulated, minimizing heat loss. Due to the high operating temperatures of the heating elements, electric furnaces are not likely to overheat. However, for this same reason, care must be taken not to exceed the safe operating temperatures of the reactor material, as these types of furnaces can easily heat the reactor walls to unsafe temperatures if not closely monitored and controlled.

Unlike electric furnaces, where heat transfer occurs due to radiation, contact electric resistive heaters are designed to transmit heat through conduction. Various form factors exist for electric resistive heaters, including band heaters, heating coils, and flexible heating cables. These contact heaters typically require external insulation to direct heat into the system. However, their use enables a reduced reactor size and cost relative to electric furnaces. Resistive heaters often contain embedded thermocouples, and, because they are in direct contact with the reactor tubing, the measured temperature closely represents the temperature of the external reactor walls. As long as the temperature in the heating element is kept below the safe temperature limit of the reactor material, the system can operate safely. To make up for the typically low maximum temperature limit of resistive heaters, a second stage heater frequently provides additional energy [50, 54 38] , 55]. The most significant drawback of this type of heater is an inability to operate at very high temperatures in sections of the reactor experiencing HTD. Typical solutions require: (i) a longer heating section or (ii) addition of an alternative heating solution for the supercritical region. For a design where cost or space are important considerations, contact resistive heaters present an economical and compact choice. A unique resistive heating approach was used in supercritical fluids heat transfer experiments in a vertical bare tube reactor in the State Scientific Centre of the Russian Federation – Institute for Physics and Power Engineering supercritical-test facility

(Obninsk, Russia). The reactor was heated by passing a current through reactor walls [56, 57]. While very efficient, this particular 4-meter vertical tube reactor consumed large amounts of electrical power due to its high reactor volume. Smaller reactors do not typically employ this form of heating.

Immersion heating refers to systems where the reactor section is immersed in a heated bath. This type of heating frequently appears in SCWO reactors, where heat may be absorbed or released in the reactor section depending on the feedstock used. Immersion heating ensures isothermal conditions and good heat transfer, but the size and cost restrictions prevent it from becoming a general solution. System thermal inertia can also present issues for some applications where a more rapid change in operating conditions is desired. Some designs utilized a hybrid approach by bringing the water to the supercritical state in the heating section and creating an isothermal environment for the reactor section. The isothermal section can be implemented with a fluidized sand bath, as utilized by the MIT reactor, a molten salt bath, as employed by a supercritical water reactor at the University of Tokyo [39], or another medium such as the fluidized alumina bath used by González et al. [40]. While less common, contact heaters can also be used as a secondary heater [23]. A summary of the heaters used by in a variety of SCWRs is shown in Table 3.

Table 3: Summary of heating methods used for SCWRs, some works use multiple reactor heating schemes and appear in two or more columns.

Contact Electric Resistive	Electric Furnace	Immersion
		Helling & Tester [18]
	Helling & Tester [18]	DiNaro et al. [21]
	Hanush et al. [23]	Cansell et al. [35]
Hanush et al. [23]	Elliot et al. [34]	Matsumura et al. [39]
Lester et al. [37]	Ramayya et al. [42]	González et al. [40]
Caputo et al. [38]	Nanda et al. [43]	Anitescu et al. [45]
Steeper et al. [41]	Molino et al. [44]	Akizuki et al. [46]
Krammer et al. [50]	Krammer et al. [50]	Thornton et al. [52]
Aida et al. [55]	Aida et al. [55]	Killilea et al. [59]
	Zhang et al. [58]	Lee et al. [60]
		Portela et al. [61]

Reagent Injection

For chemical rate studies, two mixing strategies have been reported: (i) mixing water and reagents before reaching the supercritical state, and (ii) introducing reagents into the supercritical water. In the former, the premixed water and reagents are pumped to high pressure and heated to supercritical conditions as a mixture. This is the preferred method where solid feedstocks are present, as premixing allows for solid or multiphase feedstocks, such as biomass, to reach high pressure along with the water in a single pumping solution. The second option is to keep the water and reagents separate until the water reaches the supercritical state. This post-critical injection provides fast heating of the reagents, which simplifies chemical kinetic calculations by creating a nearly isothermal reaction zone and a definitive start time for chemical reactions. The design of the mixing section and operating conditions need to be considered to optimize mixing profiles. Numerical methods can assist in the design of an effective mixer, but ambiguity in supercritical fluid properties and diffusion coefficients need to be considered [62].

A premixed slurry allows for difficult-to-pump substances, such as sewage sludge or biomasses, to form an emulsion and reach operating pressures using conventional positive displacement pumps. The water serving as a transport media for the feedstock is a practical solution for scale operations or where feedstock viscosity and the mixture heterogeneity introduce difficulty. This solution can handle fluids with high solid content; maximum particle size often depends on the ability to achieve proper seals in the pump valves. Faires in his Ph.D. dissertation describes an approach where two cylinder piston pumps with a Y-coupler are used to continuously pump a biomass/water slurry to 27 MPa at a flow rate of 5 g/s [63]. The slurry nominally contained 15% biomass solids and 85% water. The maximum particle size in the slurry was 0.84 mm, as the ground biomass particles were sieved with mesh No. 20 before mixing with water. One of the

drawbacks to pumping premixed slurries is char and tar formation, which occurs in the preheater due to hydrolysis and pyrolysis reactions that begin to occur before reaching supercritical conditions [26, 38]. Char formation can be mitigated by rapidly heating the reagents. Introducing a catalyst can also reduce char formation, although this adds significantly more process complexity [64]. Investigations of hydrothermal decomposition of organic compounds in near-critical water and at the critical transition are needed to move gasification and oxidation technology to widespread use.

In studies of chemical reaction rates, mixture heating presents a significant challenge. Reactions may occur within the heating or mixing section at non-constant temperatures, causing calculated rates to prove inaccurate in other mixing scenarios. Post-critical injection of reagents significantly reduces char formation [4, 65, 66] and provides excellent estimates for reaction residence time; however, the design of the mixing section introduces new challenges. In laboratory-scale systems with low flow rates, the high kinematic viscosity of water yields lower Reynolds numbers, resulting in laminar mixing limited by molecular diffusion. For example, the MIT reactor experienced a problem with inconsistencies in early research due to the poor mixing of water and reagent streams. When comparing methanol oxidation rates in supercritical water between the MIT reactor and other research groups, the assumption of fast-mixing was found to be inaccurate. The Reynolds number in the original MIT reactor was around 3100 corresponding the transitional (to turbulence) region and too low for consistent turbulent mixing [22]. A smaller diameter (0.25 mm) injector solved the issue by reducing the mixing time but required more complex manufacturing [67]. Larger reactors and higher flow rates promote mixing by increasing the Reynolds number. The Sandia reactor achieved Reynolds numbers greater than 19,000 through the use of larger diameter tubing and flow rates over an order of magnitude higher than the MIT reactor and did not

require a laminar mixing section [23]. In general, optimization of the operating conditions and the critical reactor dimension is required to achieve adequate mixing profiles for plug flow conditions in the reactor section. Most authors do not report on design and operation of the mixing sections, but variation in mixing profiles could be responsible for discrepancies in the literature on reported product compositions and decomposition rates [16]. The discussion related to the analysis of residence time and mixing profile uniformity is presented later in the thesis. Without knowledge of the mixing parameters, it is difficult to compare data or determine the accuracy of yield measurements, reaction rates, and chemical kinetic routes.

Reactor Monitoring, Control, and Data Acquisition

Process monitoring and control are essential for operational safety; real-time system monitoring is preferred as it allows for the safe operation of systems that may be prone to clogging, corrosion, or structural failure. Knowledge and control of temperature, pressure, residence time and chemical composition are required for chemical reaction rate studies. Some standard approaches are reported in the literature. Thermocouples can be immersed in the flow, attached to the outer walls, or embedded into sections of the reactor and then used to estimate the internal temperature. An immersed thermocouple provides the fastest temperature response and can directly measure the reactor temperatures, but direct exposure to the flow means the thermocouple must withstand the corrosive, high-temperature environment. External thermocouples bypass the issue of corrosion but respond more slowly and do not directly measure fluid temperature, so additional assumptions and calculations are required. External thermocouples can also monitor the temperature of heating elements and reactor walls to ensure that safe operating temperatures are not exceeded. A combination of internal and external thermocouples provides a good middle ground, with a few

internal thermocouples for precise temperature information and multiple external thermocouples to monitor the process at a number of locations.

Commercially available pressure sensors are not suitable for operation in supercritical water environments due to the high temperatures in the supercritical region. Typically, the pressure in the reactor system is monitored in the cold sections, such as before the heaters and after the cooling section. This approach can be readily used to monitor for flow blockages or leaks.

Residence Time

To estimate the residence time of a reaction, researchers typically assume a plug flow in the reactor section, removing the need to consider concentration gradients, fluid properties, and flow residence times at each flow cross-section. Chemical concentrations in the direction of the flow are assumed to be a function only of residence time. Residence time can be determined using only total flow rate and reactor geometry. The MIT reactor assumed a plug flow regime [18, 19], and this was later found to be a reasonable assumption that introduced a systematic error of the same magnitude as system noise even in fully laminar systems [68]. Using the plug flow assumption, residence time within the reactor can be easily determined based on the flow rate, reactor geometry, and fluid properties.

If sample analysis takes place external to the reactor, the average residence time is typically calculated. The calculations include the time fluid spent in the sampling probe, and certain corrections can be made to adjust for probe chemistry. One benefit to sampling from the supercritical environment is the fact that the reactions are likely to be quenched after the mixture undergoes rapid expansion (throttling) in the sampling probe. This assumption is often made in chemical rate studies. The sample can then be analyzed using a variety of standard *ex situ*

laboratory methods, such as HPLC, gas chromatography, mass spectrometry, or total organic carbon (TOC) analysis.

In situ monitoring

Alternatively, *in situ* analysis methods, such as Raman spectroscopy, allow chemical composition and reaction rates to be studied in real time in SCWR. The *in situ* analysis is a less common approach which requires the development and deployment of high pressure, high-temperature optical cells capable of withstanding environmental conditions and repeated heating/cooling cycles. *In situ* Raman measurements in continuous laboratory-scale reactors were first demonstrated by Sandia National Laboratories in the SFR, and more recently at reactors at the University of Tokyo [69, 70]. Other groups used diamond or other anvil cells as batch reactors, including fused-silica reactors at the Zhejiang University of Technology and the Hydrothermal Flame Reactor at Sandia [41, 71, 72]. The *in situ* analysis in the form of Raman spectroscopy allowed for extremely short residence times in continuous systems, and the SFR was capable of sampling concentrations 0.1 seconds after mixing. A shorter residence time allows for the detection of short-lived intermediate products or the determination of kinetic rates in fast reactions. The MIT reactor relied exclusively on *ex-situ* analysis methods and could only achieve a minimum residence time of six seconds. Raman spectroscopy with an excitation wavelength in the visible range is one of the most promising *in situ* process monitoring techniques for analysis of chemical composition of mixtures due to the large spectral window in water for Raman as compared to IR. The significant challenges with *in situ* Raman spectroscopy are the design of a suitable optical window and the deconvolution of the Raman signal. The optical cell in the SFR was sealed using a gold gasket, but this was found to creep due to thermal cycling and required routine maintenance to prevent leakage. The deconvolution problem presents itself when reaction intermediates are not well

known. Signals from these intermediates can become convoluted together and require significant processing to extract the concentrations of individual species. Pinkard et al. discussed the use of Raman *in situ* analysis in supercritical reactors for studies of the chemical kinetic rate in supercritical water environments [16], and the more general use of Raman spectroscopy in high temperature and high-pressure environments was summarized in a recent review [73].

CHAPTER 3: REACTOR DESIGN

Using the knowledge gained from reviewing systems in Chapter 2, the next step became designing a reactor system that would meet all the needs of this project. Because of the open-ended nature of this research, the requirements of the reactor needed to be determined prior to selecting components or materials. From the review of existing systems, an upper temperature limit of 650° C was chosen, along with a pressure limit of 35 MPa. None of the reactors reported in the literature operated at a temperature in excess of 700° C, and pressure has been shown to have a fairly weak effect relative to temperature on chemical kinetic rates [74].

Material Selection

At the temperatures and pressures of the UW system (up to 650°C and 35MPa), Inconel 625 offers superior material properties to Hastelloy C-276, although both are adequately strong to survive these conditions. All potential components should not fail due to yielding at the specified temperature and pressure, and this criterion is checked using the equation for maximum stress in a thick-walled pressure vessel below

$$\boldsymbol{\sigma_{max}} = \boldsymbol{P_i}\left(\frac{r_o^2+r_i^2}{r_o^2-r_i^2}\right) \quad (1)$$

where $\boldsymbol{\sigma_{max}}$ is the maximum stress in the pipe or tube, $\mathbf{P_i}$ is the pressure inside the tube, $\mathbf{r_o}$ is the outer radius of the tube, and $\mathbf{r_i}$ is the inner radius of the tube. This equation predicts that the

maximum stress in the reactor will be 56MPa for the reactor section (1/4” OD and wall thickness of 0.065”) and 77MPa in the heater section (1” IPS Schedule 160 Pipe). This maximum stress is then compared to the yield strength of the material to determine if failure due to yielding occurs. Inconel 625 has a yield strength of 290MPa at 650°C and a rupture strength of 365MPa at 650°C after 1000 hours. Hastelloy C-276 has a yield strength of 233MPa at 538°C. All of these failure stresses exceed the maximum stress present in the reactor, so the system will not fail due to yielding. In addition, the Inconel rupture strength is higher than the yield strength, so it will yield before rupturing. Due to its higher maximum operating temperature, Inconel 625 was determined to be superior to Hastelloy C-276. Using Inconel ensures that even in the heating section, where temperatures could easily reach 900°C, the tubing will retain an acceptable safety factor with respect to yielding. Stainless steels were not considered in the heated sections of the system due to their susceptibility to corrosion in the presence of phosphorous and chlorine [31], two elements commonly present in CWAs and CWA surrogates. For areas not experiencing elevated temperatures, 316 Stainless steel was chosen as an economical option with good corrosion resistance to a wide variety of chemicals.

Reactor Sizing

With material chosen, the size of the reactor was considered. Due to the high pressures in the system, using larger diameter tubing would require expensive thick-wall tubing. Additionally, a smaller surface to volume ratio would result from the use of larger diameter tubing, which would reduce the catalytic effect of the nickel in the reactor walls. The reactor section tubing consists of 1/4” OD tubing with 0.065” thick walls, which provide a safety factor of 2.86 with respect to yielding at maximum operating pressure. The thick-walled pressure vessel assumption in Equation 1 was used to determine the stress.

In addition to safe operating conditions, the size of the reactor contributes to the potential range of possible residence times. Large diameter tubing would result in longer residence times, while smaller diameters would accelerate the flow and result in reduced residence times. From the review, it was determined that residence times in continuous reactors tend to vary from <1 second to >180 seconds, with the SFR at Sandia National Labs covering the widest reported range [23]. Without a highly modular (high cost) system, obtaining residence times over 3 orders of magnitude is challenging, and UW reactor is designed to provide 2 orders of magnitude variation. In order to see short-lived intermediate compounds created in fast reactions, a minimum residence time of 0.5 seconds was chosen. With the 2 order of magnitude approach, this meant that the maximum residence time would ideally be around 50 seconds. To determine the residence time within the reactor, the NIST REFPROP software was used to determine the water density at a variety of temperatures. Using the principle of conservation of mass, the volumetric flow rate of the fluid in the reactor could be determined from the flow rate at the pumps prior to heating. Specific liquid injection pumps are selected based on the tubing size and desired residence times.

Pressurization

As identified in the literature review, HPLC pumps are the most common variety of pump used in continuous SCWR systems. These pumps offer precise flowrates, can operate at high pressures, and can operate in a constant flow-rate mode where the flow is independent of the pressure in the system. In combination with a back-pressure regulator, this allows the pressure and flow rate to be controlled independently. The HPLC pumps used in the UW SCWR system are an LD Class (dual piston) pump and an LS Class (single piston) pump from Teledyne SSI. The LD-036 pump controls the flow rate of water into the system and can operate at flow rates from 0.01 to 36 mL/min at pressures up to 6000 psi. At flow rates below 0.80 mL/min, the flow accuracy decreases to greater

than 2% of the set point, restricting the effective range of the pump. The LS-005 pump injects reagents into the system and can operate at flow rates from 0.001 to 5 mL/min with an upper pressure limit of 6000 psi. This smaller pump maintains accuracy of 0.2% across all flow rates. Both pumps are equipped with leak sensors, pulse dampeners, and pressure sensors to ensure safe and consistent operation.

Heaters

With the flow rates and system size established, the heat supply for the system must next be determined. As discussed in Chapter 2, the most common heating solutions are fluidized bed heaters, radiative furnaces, and conductive heaters. The amount of heat necessary to bring water from room temperature up to supercritical conditions was estimated using the maximum mass flow rate of the water and the change in enthalpy from room temperature to supercritical conditions. This is shown in equation 2 below

$$\dot{\boldsymbol{Q}} = \dot{\boldsymbol{m}}(\boldsymbol{h_{max}} - \boldsymbol{h_{min}}) \tag{2}$$

where $\dot{\boldsymbol{Q}}$ is the power required, in kilowatts, $\dot{\boldsymbol{m}}$ is the mass flow rate, in kilograms per second, and $\boldsymbol{h_{max}}$ and $\boldsymbol{h_{min}}$ are the specific enthalpies at supercritical conditions and ambient conditions, respectively. The maximum heat was determined using a maximum flow rate of 41 mL/min (the sum of the maximum flow rates of both pumps) and an operating condition of 25MPa and 650°C at the heater exit. The enthalpies were taken from REFPROP. For this operating condition, the water must absorb a maximum of 2.467 kW of heat.

Two potential heating solutions have been identified: tube furnaces and coil heaters. The pros and cons of each method are considered below. In general, the coil heaters provide a more affordable heating solution with a faster response time at the expense of maximum operating temperature and flexibility, while tube furnaces can operate at higher temperatures and accommodate long coils of tubing but react slowly to changes to the temperature set point.

Table 4: Summary of the advantages and disadvantages of coil heaters and tube furnaces.

Coil Heaters		Tube Furnaces	
Pros	Cons	Pros	Cons
• Compact • Rapidly achieves the desired temperature	• Maximum temperature ~ 820°C • Requires large OD tubing	• Maximum temperature ~ 950°C • Works with coiled tubing	• Slow to reach desired temperatures • Large

The most appropriate coil heater for this application was found to be the Tempco Mighty-Band line of coil heaters. These heaters offer Inconel construction, operating temperatures up to 816°C, and a relatively small minimum ID of 19 mm. The first iteration of the heating system used two of these heaters in series around a 61 cm section of 19 mm OD tubing. This configuration provided rapid heat-up times but was unable to reach temperatures significantly above the critical point of water. The reason for this was determined to be the heat transfer crisis, which was discussed in Chapter 2. The need for an alternative configuration in the heating section was identified from the calculations used to generate Figure 5. Due to the inefficient transfer of heat from hot tube walls into the fluid, operating the heaters at higher temperatures had a minor effect on the temperature at the exit of the heating section.

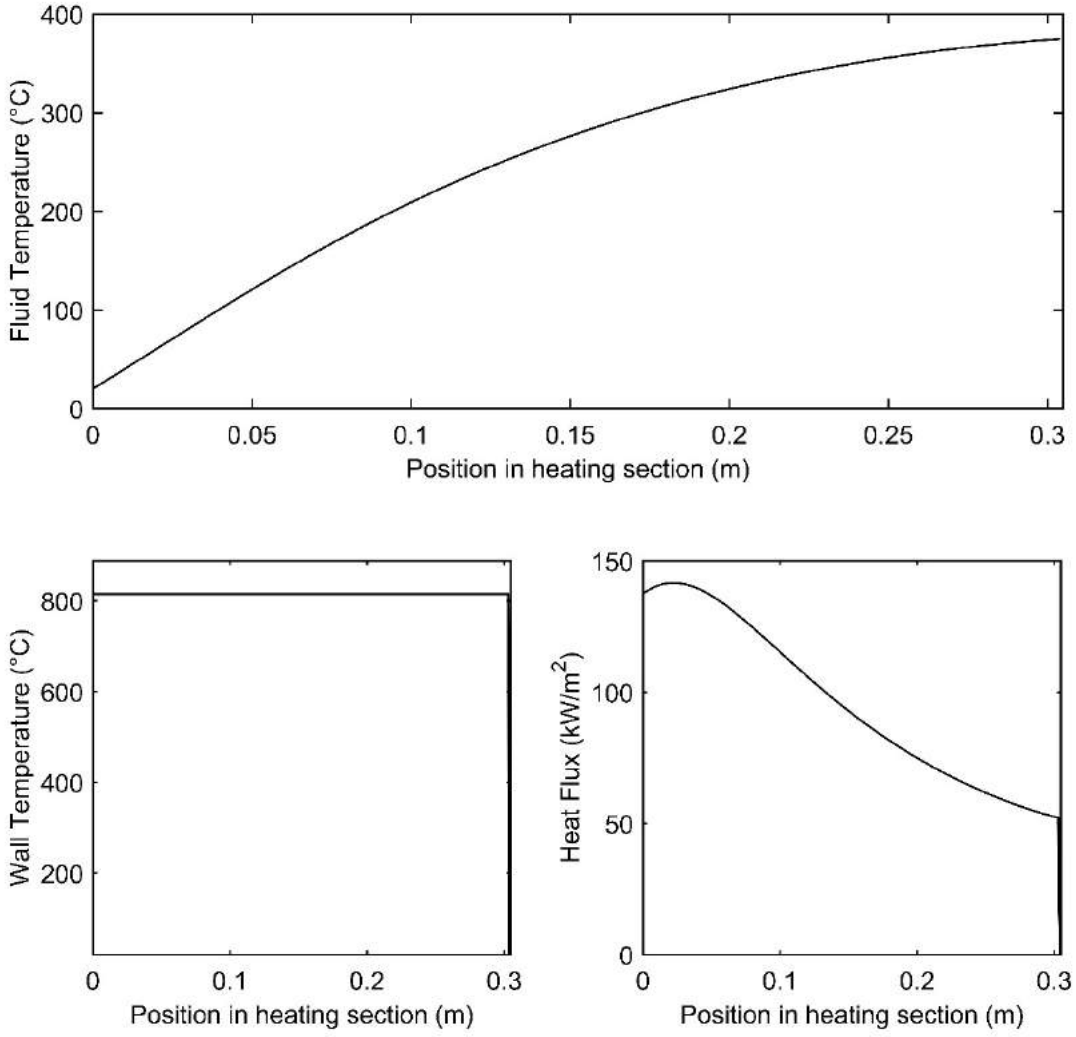

Figure 5: Fluid temperature, wall temperature, and heat flux vs position in the heating section for the original heat configuration of two 2000 W coil heaters with a combined length of 61 cm coiled around a tube with a 19 mm outer diameter. To approximate a worst-case scenario, the assumption of a constant Nusselt number of 3.66 (constant wall temperature) is assumed. The heaters are assumed to be perfectly insulated and operating at maximum temperature.

If a long coil of small diameter tubing were instead used, the fluid would be able to reach the wall temperature despite the poor heat transfer inherent to supercritical temperatures. This configuration would require the use of a tube furnace, and an OMEGALUX CRFC (Ceramic Radiant Full Cylinder) furnace heater was chosen to do the job. These heaters have a maximum operating temperature of 982°C and provide the heat necessary to reach temperatures well above the critical point. Inside the furnace is a 6.1 m coil of 6.35 mm OD tubing. By using a longer length of smaller diameter coil, the surface to area ratio is drastically increased without sacrificing residence time within the heater. This configuration enables the design temperature of 650°C to be achieved easily, as shown in Figure 6.

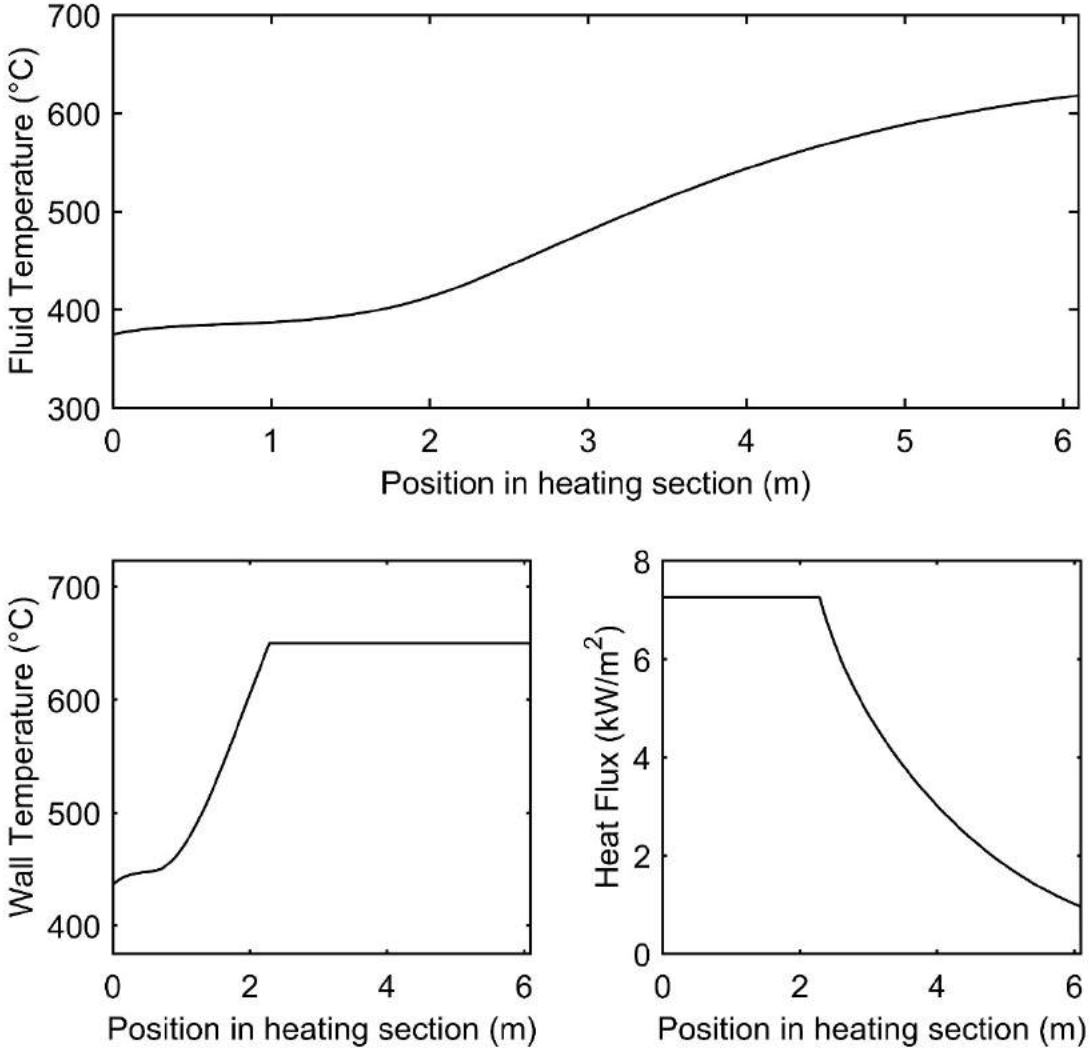

Figure 6: Heater performance with a 6.1 m coil of 6.35 mm OD tubing. The input temperature for this scenario is the output temperature of a single Mighty-Band heater from the previous scenario. The heater in this scenario is set to 650°C, as the exit temperature will nearly match the heater temperature up to the operational limit. The Nusselt number is assumed to be constant at 3.66 to err on the conservative side.

The final heat configuration uses a combination of coil heaters and tube furnaces. A 2000 W Tempco Mighty-Band coil heater with thermocouple comes first, and this heater provides heat into the system through conduction. The heater measures 30.5 cm in length and is coiled around a 19 mm OD tube of Inconel 625. The heater is made of Inconel 600 with a supply voltage of 240 V. An embedded thermocouple provides the temperature at the end of the coil. The second heater is an 1800 W OMEGALUX CRFC (Ceramic Radiant Full Cylinder) furnace heater. This heater has a maximum operating temperature of 982°C and provides the heat necessary to reach temperatures well above the critical point. Inside the furnace is a 6.1 m long coil of 6.35 mm OD tubing. Testing of this configuration has confirmed the ability to operate the reactor at temperatures up to 650°C at the exit of the heating section.

In addition to the primary heating system, two small make-up heaters keep the reactor section at the set temperature. The first of these heaters is a small, low-wattage flexible cable heater. This heater is wrapped around the mixing section and keeps the system from losing heat upon exiting the primary heaters. The second heater is a 700 W OMEGALUX CRFC that contains the coiled reactor section and provides an isothermal reaction environment. Both heaters are used only to compensate for heat loss in the reactor section and are not designed to provide significant heat into the system.

Cooling System

After exiting the reactor section, the fluid is cooled and depressurized to safe temperatures and pressures. The design of the heat exchanger is primarily driven by three parameters: the maximum temperature within the system, the maximum allowable temperature at the back-pressure regulator, and the flow rate of the system. The plastic diaphragm in the back-pressure regulator has a maximum operating temperature of 150°C, so the heat exchanger must be capable of dropping the

temperature below this value. To avoid a phase change across the back-pressure regulator, a desired maximum temperature of 100°C was chosen for effluent leaving the heat exchanger. Like the rest of the system, the heat exchanger must withstand pressures of up to 35 MPa and temperatures of up to 650°C and must possess excellent resistance to corrosion. Surfaces exposed to near-supercritical water experience the most corrosion in continuous SCWR systems, making the heat exchanger one of the most susceptible components to corrosion [26]. For this reason, Inconel 625 was required for the process side of the heat exchanger.

The initial heat exchanger chosen for the project was a Graham Heliflow 8SP-10 heat exchanger with Inconel 625 tubes and manifolds and a cast steel shell. These heat exchangers have the advantage of having been used for supercritical applications in the past along with a high operational pressure. During operation without reagents, this heat exchanger was capable of cooling the supercritical water to well below 100°C with a closed-loop cooling system. However, when reactive reagents were introduced, cooling led to phase separation (gas versus liquid). The design of this heat exchanger caused the gases to become trapped inside the heat exchangers coils, and these are periodically shed into the exchanger effluent. This was confirmed by taking a large number of samples over a short time period to see if the signal varied drastically over a short period of time. To accomplish this, 100 spectra were taken, each with an integration time of 100 ms and no averaging. This resulted in noisy data, but the results shown in Figure 7 confirm the presence of hydrogen bubbles in the effluent.

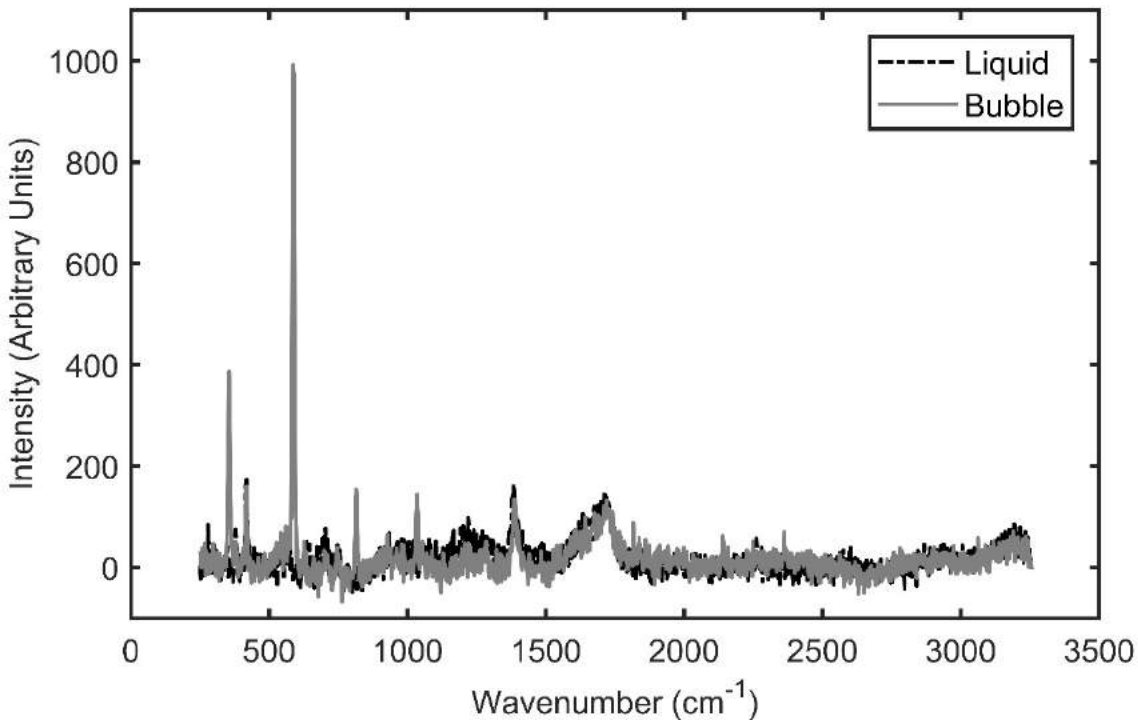

Figure 7: Evidence of bubbles in the region downstream of the heat exchanger. The 4 large peaks present in the bubble signal are the 4 characteristic peaks of hydrogen. Both spectra were taken consecutively with a 100 ms integration time.

While the formation of bubbles did not affect the heat exchanger's ability to cool the reactor effluent, trapping reaction products invalidates the assumption of constant mass-flow throughout the system and makes accurate measurements of product composition impossible at any locations downstream of the heat exchanger. Additionally, for reagents that decompose into hydrogen or other flammable gases, a pressurized pocket of gas presents a significant safety risk in the case of a leak in the inner tube. For these reasons, a new heat exchanger must be sourced with a design that prevents the trapping of insoluble gases.

Controls and Monitoring

Control of the reactor is provided through several different systems, all of which are independently controlled. While a closed-loop control scheme would be more efficient in the long run, implementing such a control scheme proved difficult and would require a considerable time investment. For this reason, and to ensure safe operation of the reactor at all times, the controls remain independent. The flow rates of the reagent and the water are controlled through the pump driver software on a computer, and the setpoint is specified in milliliters per minute. This flow rate is taken at ambient temperature and can be used to determine flow rates in the hot sections of the reactor. Pressure is controlled with the back-pressure regulator with a set-point determined by a high-pressure nitrogen bottle. The nitrogen bottle can supply pressures as high as 35 MPa, but typically is held to 25 MPa during normal operation. Temperature and flow rate within the system are controlled by the heaters and pumps, respectively, which are described in more detail in their respective sections.

CHAPTER 4: RAMAN SPECTROSCOPY

To determine the chemical kinetic rates in supercritical water, time-resolved information about chemical concentration and composition is required. This information is typically determined using samples drawn off from the reactor and rapidly quenched. Analyzing samples does provide useful information about reaction yields but not the rates of reaction. To address this issue, *in situ* approaches to chemical composition data were investigated, and Raman spectroscopy was identified as the most suitable *in situ* method for supercritical water. Raman spectroscopy is particularly useful in supercritical water due to the relative transparency of water and the high-pressure environment. Raman signal scales linearly with pressure, so the supercritical pressures alleviate the issue of weak signals from gaseous species.

Optical Cell

To use Raman spectroscopy in a supercritical environment, optical access to the reactor interior is required. An optical cell of some sort is typically used for this, but the high pressure and temperature of a supercritical water reactor pose a significant challenge with respect to the design of such a cell. For this application, a custom optical cell from MarqMetrix is used. The optical cell features a spherical sapphire lens and an Inconel 625 construction with High Pressure LF4 connections. The first optical cell used on the reactor could easily withstand operational pressures in the ambient temperature, but the sapphire lens cracked during the reactor heating due to thermal expansion when the system reached temperatures above 300° C. As a short-term solution, the optical cell was moved downstream of the heat exchanger, but this introduced residence time uncertainty and inconsistent signals due to insoluble gasses becoming trapped in the heat exchanger. To resolve this issue, a modified optical cell designed to accommodate thermal expansion was built. This optical cell is located upstream of the heat exchanger and immediately after the reactor coil and has successfully operated at pressures up to 25 MPa with a simultaneous temperature of 380° C.

Signal Processing

One of the primary challenges related to processing Raman signals in water is the subtraction of the baseline signal associated with fluorescence. Peak parameters normally used for comparison, such as height, area, and width, cannot be accurately extracted without first subtracting this baseline signal. Many methods exist to accomplish this subtraction, and several were compared for their suitability to our system.

Modified Polyfit Subtraction

The first method of baseline subtraction used was the modified polyfit method [75]. This method uses a polynomial fit with the constraint that if a point on the fitted curve has a greater intensity than the same point on the spectra, the value of that point is set to the value of the original spectra at the corresponding wavenumber. The resulting curve is then fit again, and the process is iterated until the resulting curve lies fully below the spectra. Using this method has the advantage of eliminating negative intensities, and the methodology behind the technique is simple enough to be adapted to any convenient programming language. An example of this technique is shown in Figure 8. The method was applied to a sample of 25% ethanol in water, with 100 iterations and a 5^{th} order fitting polynomial.

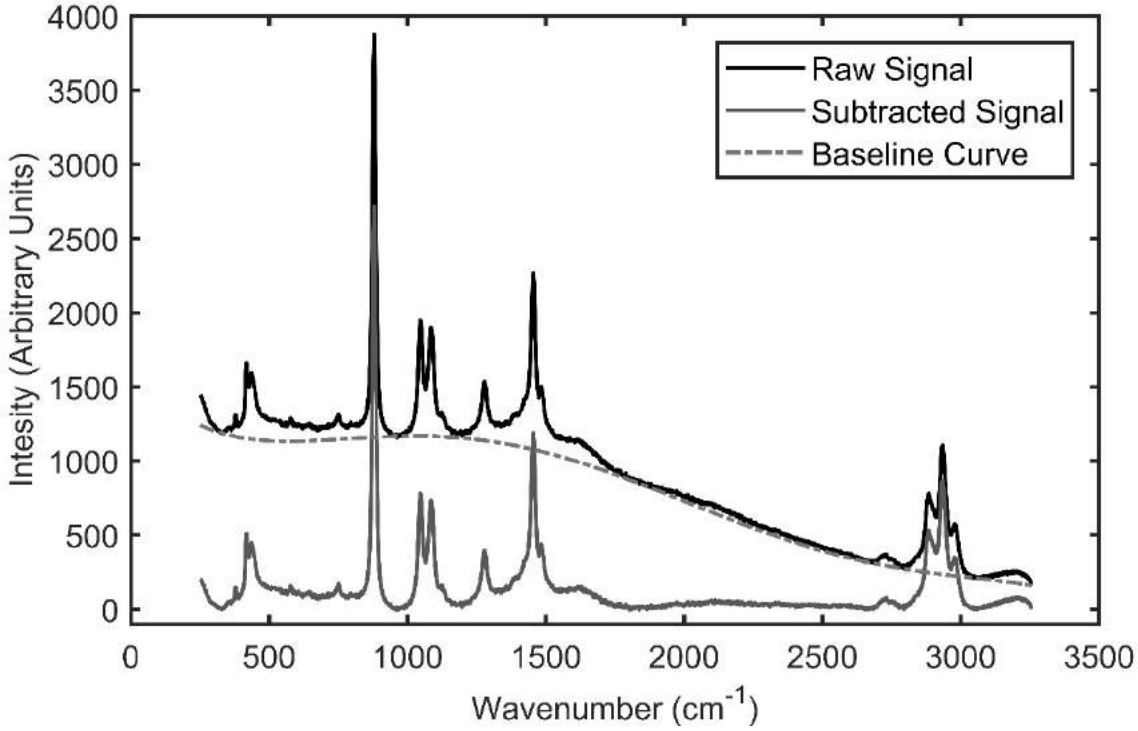

Figure 8: Modified polyfit method applied to the Raman spectra of 25% ethanol in water. This figure was generated using 100 iterations and a 5th order polynomial function. The original spectra, fitted baseline, and baseline subtracted signal are all shown.

While the modified polynomial method provides satisfactory results when applied to single spectra, attempting to apply the method to a wide variety of spectra creates significant discrepancies. Changing the number of iterations or order of the polynomial can help improve the fit of individual spectra, but this creates inconsistencies when comparing data. For this reason, alternative baseline subtraction methods were investigated.

Wavelet Method

A wavelet algorithm with built-in peak detection and background fitting was investigated [76]. This method proved capable of subtracting the baseline data from a wide variety of input signals

but ran into difficulties with the processing of particularly short or wide peaks. As shown in Figure 9, this method creates a much more accurate baseline in the lower wavenumber range of 500-1500 cm^{-1} but truncates part of the peaks in the high wavenumber range. In addition, due to the complicated nature of the algorithm, this code works much more as a "black box" than the much simpler modified polynomial method. Finally, the algorithm for this method is programmed in the language R, while other processing tools work within the MATLAB environment. This complicated processing technique makes is challenging to use for proof-of-concept studies, however, the method can be tuned to perform the automated analysis.

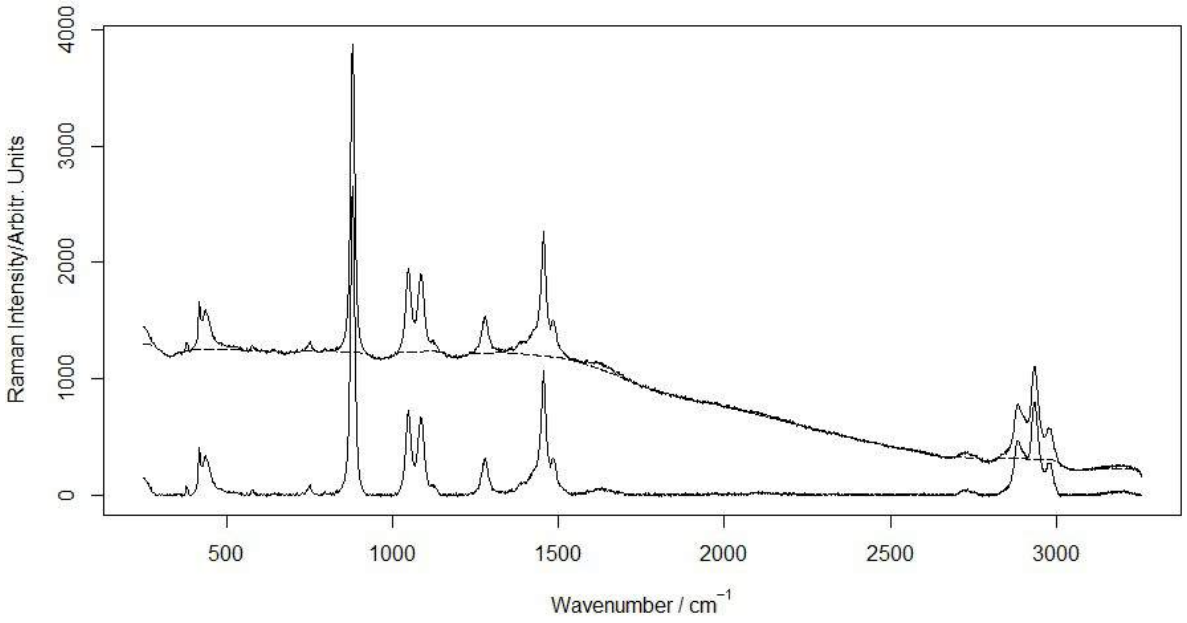

Figure 9: Baseline subtraction using the wavelet algorithm described by Hang et al. This figure was generated with a 25% Ethanol in water signal and a lambda value of 1000.

Manual Baseline Subtraction

After evaluating multiple automatic baseline subtraction methods, we evaluated manual baseline subtraction method. For this task, the graphing software was used to snap a baseline to

user-defined points fit the baseline for a specific spectrum. This method provided the most control over the subtraction process and created an accurate baseline and the processed spectra, however, the method is time-consuming and can lead to discrepancies between signals if the user failed to specify identical points on different data files. An example of a curve with a user-defined baseline is shown in Figure 10.

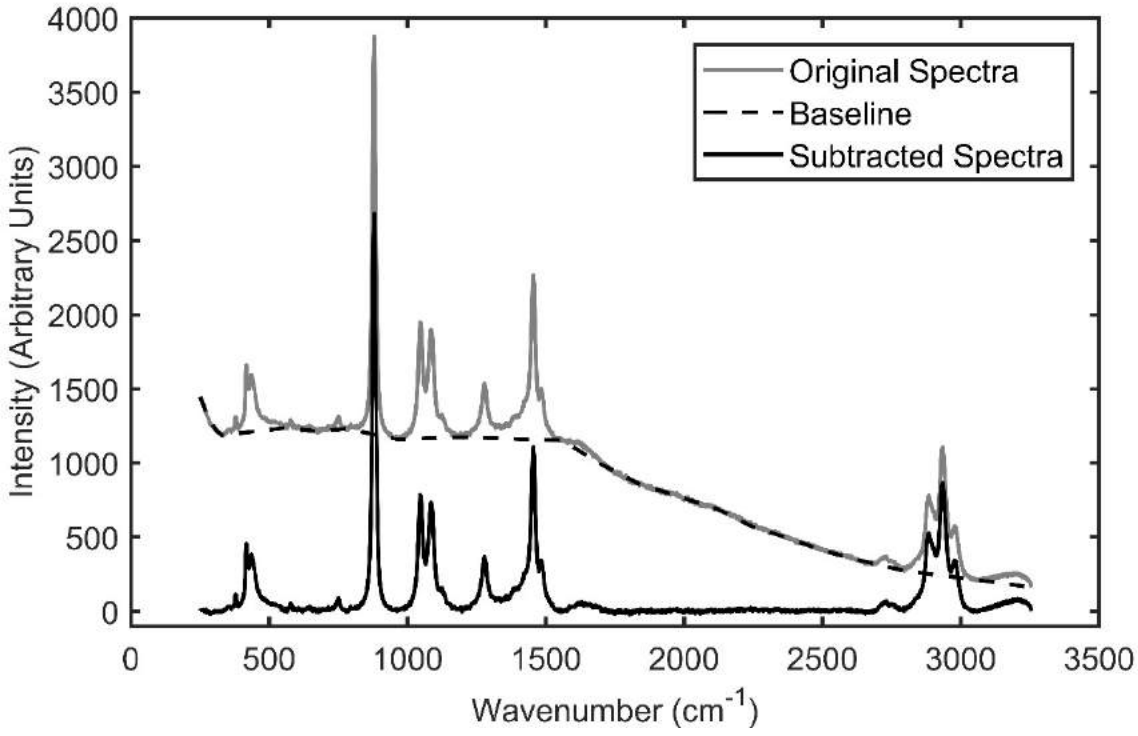

Figure 10: Manual baseline subtraction method created using user-defined anchor points and a linear interpolation between points. The sample is 25% ethanol in water

While the manual method is easy to use and can produce data with a better fit than both the modified polyfit and wavelet methods (with default coefficients), the time required to process large numbers of data prevents it from becoming a viable method for subtracting baseline signal.

Semi-Manual Method

After evaluating automated and manual baseline subtraction, the concept of a semi-manual baseline subtraction method was proposed. This method functions similarly to the manual subtraction method in that a user defines the anchor points for the baseline, but the defined points are used to automatically process all datasets involving the same chemical constituents. For example, if data for ethanol were gathered at various concentrations, residence times, and temperatures, the semi-manual technique would require only a single set of baseline points to be manually generated to fit all data relating to ethanol decomposition. The process of selecting baseline anchor points must be repeated for each new reagent to ensure that no baseline points fall inside of peaks. For reagents with many peaks, defining an appropriate set of anchor points may prove difficult, but this is true for other methods of baseline subtraction as well. If applied to the same spectra as the previous figures, this method provides a signal identical to manual baseline subtraction, see Figure 10. To show its ability to handle multiple spectra, this method is for formic acid analysis at 1%, 2.5%, and 5% concentration in Figure 11.

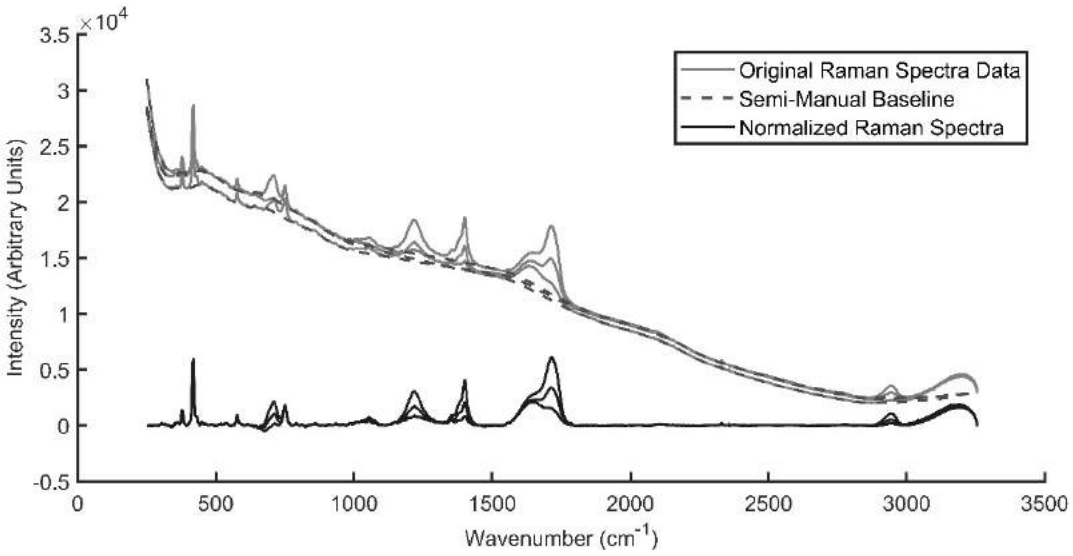

Figure 11: Formic acid at 1%, 2.5%, and 5% concentration plotted with each generated baseline and the subtracted baseline. The semi-manual method looks identical to the manual method on ethanol data, so formic acid was chosen to show how the method works when applied to data with varying chemical concentrations.

With the reactor built and all components tested at pressure and temperature, Raman spectra could be collected for any number of reagents. Preliminary experiments included methanol, ethanol, isopropyl alcohol, glucose, and formic acid. For each compound, the raw spectra are collected, processed to subtract the baseline signal, and used to determine chemical concentration. In order to acquire detailed chemical kinetic rates, baseline spectra must be collected to relate peak characteristics and chemical concentrations. These baseline data can be acquired for liquids that dissolve completely in water but is more challenging to acquire for insoluble fluids. Additionally, some reagents decompose into a wide variety of products, significantly complicating the use of Raman spectroscopy for species identification. An example of this is glucose, which decomposes rapidly into a large number of intermediates [16]. The signal of pure glucose is compared to the signal obtained from the reactor effluent in Figure 12.

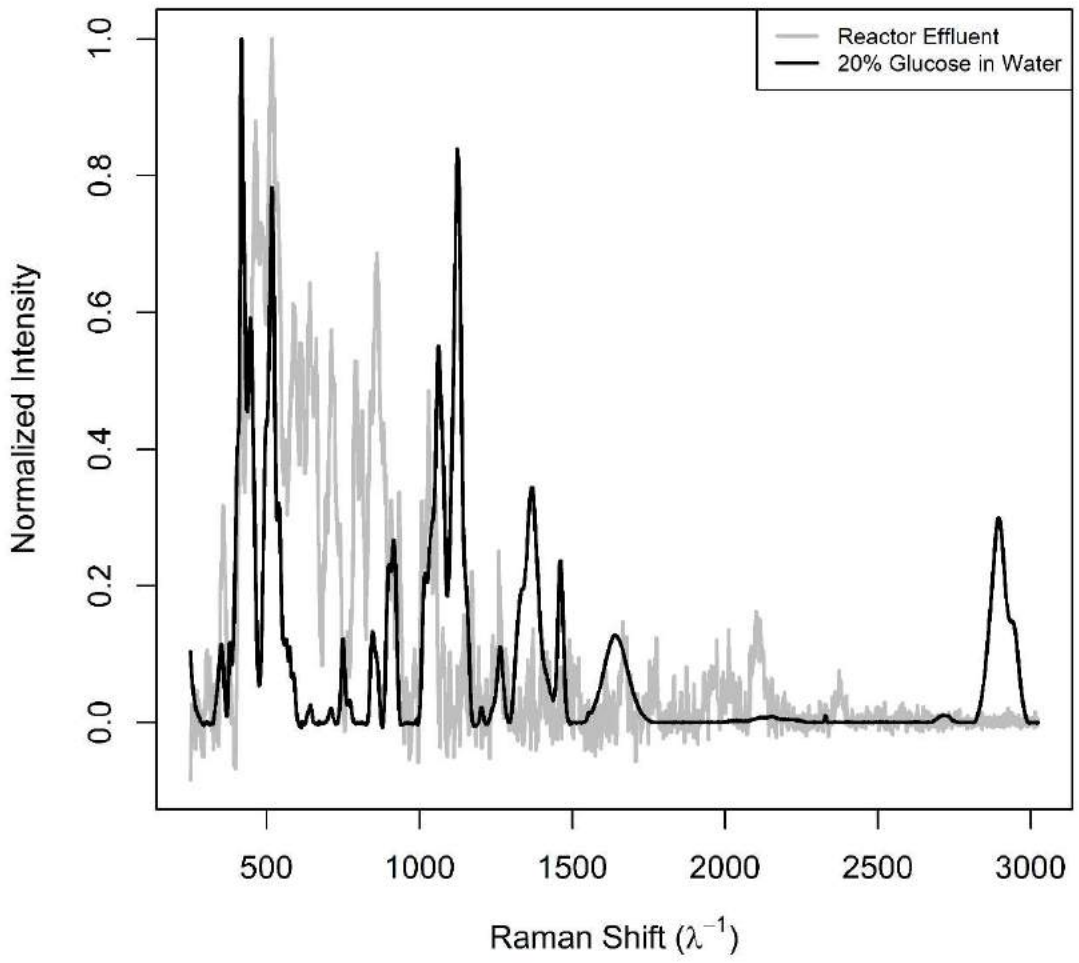

Figure 12: The Raman spectrum of glucose compared to the spectrum observed from the reactor effluent with glucose as the reagent. While the effluent is clearly not glucose, little else can be determined from the crowded signal.

Determining chemical composition, let alone concentration, from such a complicated signal is difficult. At a minimum, deconvoluting the signal into individual components would require knowledge of all potential compounds that would be expected to appear during glucose gasification. For this reason, Raman spectroscopy is best suited to compounds with relatively

simple reaction pathways, or at least compounds where the mechanisms of decomposition are relatively simple.

In contrast to glucose, formic acid decomposes via two relatively simple pathways and produces a small number of products. As can be seen in Figure 13, formic acid and its products form clear, distinct peaks and can be easily identified without extensive processing. Formic acid is a much simpler compound than glucose, making it well suited for Raman spectroscopy. One challenge is that formic acid decomposes slowly into carbon dioxide at room temperature, which can cause problems with the vapor locking in the feed line in which event purging of pumping subsystem is required if a bubble enters the pump head. With the exception of this minor inconvenience, formic acid serves as a good test compound due to its simple chemistry, clean Raman signal, and rapid reactions at relatively low temperatures.

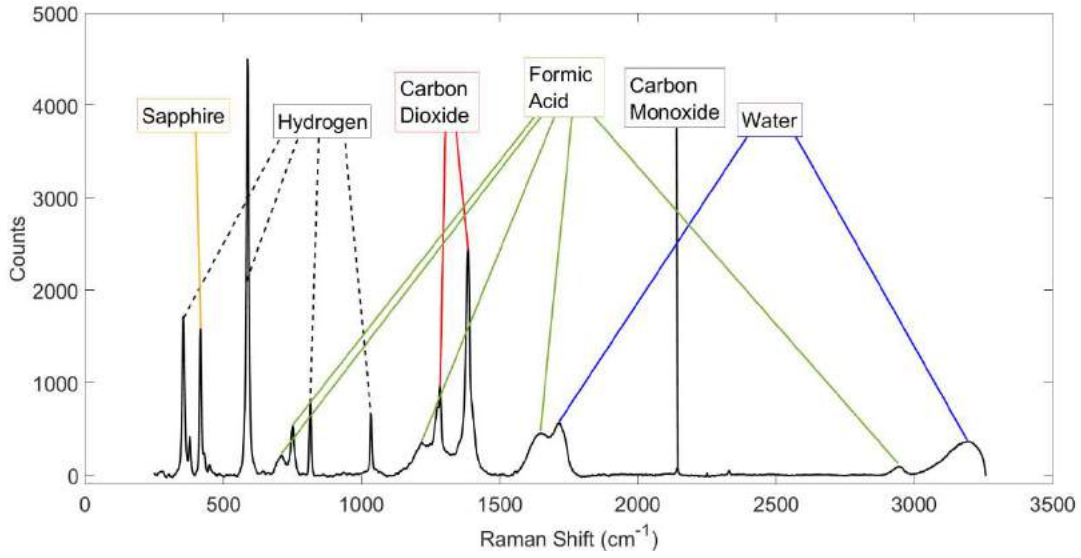

Figure 13: Effluent signal of formic acid in water, along with products and their corresponding peaks. Peaks and compounds were correlated using spectral libraries.

CONCLUSIONS AND FUTURE WORK

While research into chemical kinetic rates for organic compounds has only just begun using the UW SCWR reactor, the reactor will enable a wide variety of experiments to be conducted during the remainder of the project. Through the extensive review of existing systems and incorporation of new and promising technologies such as Raman spectroscopy, the reactor will provide insight into decomposition reactions in real time. The reactor has been shown to work across the intended operational space with the possibility of future modification to expand the range of possible parameters. Future work will include the determination of chemical kinetic rates for formic acid, alcohols like methanol, ethanol, and isopropyl alcohol, and toxic chemical agent surrogates such as DMMP. The reactor has been designed to accommodate oxidation studies. The Raman processing techniques discussed in this manuscript enables the rapid and consistent processing of large datasets. The UW SCWR enables the study of a wide variety of supercritical water reactions, and the research conducted during its design provides a framework for future studies and reactors at UW.

REFERENCES

[1] Hodes, M., Marrone, P. A., Hong, G. T., Smith, K. A., and Tester, J. W., 2004, "Salt precipitation and scale control in supercritical water oxidation—Part A: fundamentals and research," The Journal of Supercritical Fluids, 29(3), pp. 265-288.

[2] Lemmon, E. W., Huber, M. L., and McLinden, M. O., 2013, "NIST Standard Reference Database 23: Reference Fluid Thermodynamic and Transport Properties-REFPROP, Version 9.1, National Institute of Standards and Technology."

[3] Wagner, W., and Pruß, A., 2002, "The IAPWS Formulation 1995 for the Thermodynamic Properties of Ordinary Water Substance for General and Scientific Use," Journal of Physical and Chemical Reference Data, 31(2), pp. 387-535.

[4] Reddy, S. N., Nanda, S., Dalai, A. K., and Kozinski, J. A., 2014, "Supercritical water gasification of biomass for hydrogen production," International Journal of Hydrogen Energy, 39(13), pp. 6912-6926.

[5] Kruse, A., 2009, "Hydrothermal biomass gasification," 20th Year Anniversary Issue of the Journal of Supercritical Fluids, 47(3), pp. 391-399.

[6] Savage, P. E., Gopalan, S., Mizan, T. I., Martino, C. J., and Brock, E. E., 1995, "Reactions at supercritical conditions: Applications and fundamentals," AIChE Journal, 41(7), pp. 1723-1778.

[7] Savage, P. E., 1999, "Organic Chemical Reactions in Supercritical Water," Chemical Reviews, 99(2), pp. 603-622.

[8] Svanström, M., Fröling, M., Modell, M., Peters, W. A., and Tester, J., 2004, "Environmental assessment of supercritical water oxidation of sewage sludge," Resources, Conservation and Recycling, 41(4), pp. 321-338.

[9] Bermejo, M. D., and Cocero, M. J., 2006, "Supercritical water oxidation: A technical review," AIChE Journal, 52(11), pp. 3933-3951.

[10] Antal, M. J., Allen, S. G., Schulman, D., Xu, X., and Divilio, R. J., 2000, "Biomass Gasification in Supercritical Water," Industrial & Engineering Chemistry Research, 39(11), pp. 4040-4053.

[11] Kamler, J., and Soria, J. A., 2012, "Supercritical Water Gasification of Municipal Sludge: A Novel Approach to Waste Treatment and Energy Recovery," Gasification for Practical Applications, Y. Yun, ed., InTech, Rijeka, pp. Ch.-06.

[12] Gong, M., Nanda, S., Romero, M. J., Zhu, W., and Kozinski, J. A., 2017, "Subcritical and supercritical water gasification of humic acid as a model compound of humic substances in sewage sludge," The Journal of Supercritical Fluids, 119, pp. 130-138.

[13] Wang, C., Zhu, W., Gong, M., Su, Y., and Fan, Y., 2017, "Influence of H2O2 and Ni catalysts on hydrogen production and PAHs inhibition from the supercritical water gasification of dewatered sewage sludge," J. Supercrit. Fluids, 130, pp. 183-188.

[14] Zhang, L., Champagne, P., and Xu, C., 2011, "Screening of supported transition metal catalysts for hydrogen production from glucose via catalytic supercritical water gasification," European Fuel Cell 2009, 36(16), pp. 9591-9601.

[15] Yu, J., Chen, Q., Guan, Q., Li, B., Ning, P., Gu, J., and Lu, X., 2016, "Characterization of the liquid intermediates from gasification of lignite in supercritical water: Insights into the gasification process for hydrogen production," International Journal of Hydrogen Energy, 41(39), pp. 17309-17322.

[16] Pinkard, B. R., Gorman, D. J., Tiwari, K., Kramlich, J. C., Reinhall, P. G., and Novosselov, I. V., 2018, "Review of Gasification of Organic Compounds in Continuous-Flow, Supercritical Water Reactors," Industrial & Engineering Chemistry Research.

[17] DiLeo, G. J., and Savage, P. E., 2006, "Catalysis during methanol gasification in supercritical water," The Journal of Supercritical Fluids, 39(2), pp. 228-232.

[18] Helling, R. K., and Tester, J. W., 1987, "Oxidation kinetics of carbon monoxide in supercritical water," Energy & Fuels, 1(5), pp. 417-423.

[19] Helling, R. K., and Tester, J. W., 1988, "Oxidation of simple compounds and mixtures in supercritical water: carbon monoxide, ammonia and ethanol," Environmental Science & Technology, 22(11), pp. 1319-1324.

[20] Webley, P. A., and Tester, J. W., "Fundamental Kinetics and Mechanistic Pathways for Oxidation Reactions in Supercritical Water," SAE International.

[21] DiNaro, J. L., Tester, J. W., Howard, J. B., and Swallow, K. C., 2000, "Experimental measurements of benzene oxidation in supercritical water," AIChE Journal, 46(11), pp. 2274-2284.

[22] Helling, R. K., 1986, "Oxidation Kinetics of Simple Compounds in Supercritical Water: Carbon Monoxide, Ammonia and Ethanol," MIT.

[23] Hanush, R. G., Rice, S. F., Hunter, T. B., and Aiken, J. D., 1995, "Operation and performance of the Supercritical Fluids Reactor (SFR)," United States.

[24] Boyd, W. K., and Pray, H. A., 1957, "Corrosion of Stainless Steels In Supercritical Water," CORROSION, 13(6), pp. 33-42.

[25] Coriou, H., Grall, L., MahlEu, C., and Pelas, M., 1966, "Sensitivity to Stress Corrosion and Intergranular Attack of High-Nickel Austenitic Alloys," CORROSION, 22(10), pp. 280-290.

[26] Marrone, P. A., and Hong, G. T., 2009, "Corrosion control methods in supercritical water oxidation and gasification processes," The Journal of Supercritical Fluids, 51(2), pp. 83-103.

[27] Kritzer, P., 2004, "Corrosion in high-temperature and supercritical water and aqueous solutions: a review," The Journal of Supercritical Fluids, 29(1), pp. 1-29.

[28] Thomason, T. B., and Modell, M., 1984, "Supercritical Water Destruction of Aqueous Wastes," Hazardous Waste, 1(4), pp. 453-467.

[29] Tester, J. W., Holgate, H. R., Armellini, F. J., Webley, P. A., Killilea, W. R., Hong, G. T., and Barner, H. E., 1993, "Supercritical Water Oxidation Technology," Emerging Technologies in Hazardous Waste Management III, American Chemical Society, pp. 35-76.

[30] Marrone, P. A., Cantwell, S. D., and Dalton, D. W., 2005, "SCWO System Designs for Waste Treatment: Application to Chemical Weapons Destruction," Industrial & Engineering Chemistry Research, 44(24), pp. 9030-9039.

[31] Tang, X., Wang, S., Qian, L., Li, Y., Lin, Z., Xu, D., and zhang, Y., 2015, "Corrosion behavior of nickel base alloys, stainless steel and titanium alloy in supercritical water containing chloride, phosphate and oxygen," Chemical Engineering Research and Design, 100, pp. 530-541.

[32] National Research, C., 2001, Analysis of Engineering Design Studies for Demilitarization of Assembled Chemical Weapons at Pueblo Chemical Depot, The National Academies Press, Washington, DC.

[33] National Research, C., 2002, Analysis of Engineering Design Studies for Demilitarization of Assembled Chemical Weapons at Blue Grass Army Depot, The National Academies Press, Washington, DC.

[34] Elliott, D. C., Phelps, M. R., Sealock, L. J., and Baker, E. G., 1994, "Chemical Processing in High-Pressure Aqueous Environments. 4. Continuous-Flow Reactor Process Development Experiments for Organics Destruction," Industrial & Engineering Chemistry Research, 33(3), pp. 566-574.

[35] Cansell, F., Beslin, P., and Berdeu, B., 1998, "Hydrothermal oxidation of model molecules and industrial wastes," Environmental Progress, 17(4), pp. 240-245.

[36] Benjumea, J. M., Sánchez-Oneto, J., Portela, J. R., and Martínez de la Ossa, E. J., 2017, "Temperature control in a supercritical water oxidation reactor: Assessing strategies for highly concentrated wastewaters," The Journal of Supercritical Fluids, 119, pp. 72-80.

[37] Lester, E., Blood, P., Denyer, J., Giddings, D., Azzopardi, B., and Poliakoff, M., 2006, "Reaction engineering: The supercritical water hydrothermal synthesis of nano-particles," The Journal of Supercritical Fluids, 37(2), pp. 209-214.

[38] Caputo, G., Rubio, P., Scargiali, F., Marotta, G., and Brucato, A., 2016, "Experimental and fluid dynamic study of continuous supercritical water gasification of glucose," The Journal of Supercritical Fluids, 107, pp. 450-461.

[39] Matsumura, Y., Nunoura, T., Urase, T., and Yamamoto, K., 2000, "Supercritical water oxidation of high concentrations of phenol," Journal of Hazardous Materials, 73(3), pp. 245-254.

[40] González, G., Salvadó, J., and Montané, D., 2004, "Reactions of vanillic acid in sub- and supercritical water," The Journal of Supercritical Fluids, 31(1), pp. 57-66.

[41] Steeper, R. R., Rice, S. F., Brown, M. S., and Johnston, S. C., 1992, "Methane and methanol diffusion flames in supercritical water," The Journal of Supercritical Fluids, 5(4), pp. 262-268.

[42] Ramayya, S., Brittain, A., DeAlmeida, C., Mok, W., and Antal, M. J., 1987, "Acid-catalysed dehydration of alcohols in supercritical water," Fuel, 66(10), pp. 1364-1371.

[43] Nanda, S., Reddy, S. N., Hunter, H. N., Dalai, A. K., and Kozinski, J. A., 2015, "Supercritical water gasification of fructose as a model compound for waste fruits and vegetables," The Journal of Supercritical Fluids, 104, pp. 112-121.

[44] Molino, A., Migliori, M., Macrì, D., Valerio, V., Villone, A., Nanna, F., Iovane, P., and Marino, T., 2016, "Glucose gasification in super-critical water conditions for both syngas production and green chemicals with a continuous process," Renewable Energy, 91, pp. 451-455.

[45] Anitescu, G., Zhang, Z., and Tavlarides, L. L., 1999, "A Kinetic Study of Methanol Oxidation in Supercritical Water," Industrial & Engineering Chemistry Research, 38(6), pp. 2231-2237.

[46] Akizuki, M., Tomita, K., and Oshima, Y., 2011, "Kinetics of solid acid catalyzed 1-octene reactions with TiO2 in sub- and supercritical water," The Journal of Supercritical Fluids, 56(1), pp. 14-20.

[47] Sasaki, M., Kabyemela, B., Malaluan, R., Hirose, S., Takeda, N., Adschiri, T., and Arai, K., 1998, "Cellulose hydrolysis in subcritical and supercritical water," The Journal of Supercritical Fluids, 13(1–3), pp. 261-268.

[48] Middelkoop, V., Tighe, C. J., Kellici, S., Gruar, R. I., Perkins, J. M., Jacques, S. D. M., Barnes, P., and Darr, J. A., 2014, "Imaging the continuous hydrothermal flow synthesis of nanoparticulate CeO2 at different supercritical water temperatures using in situ angle-dispersive diffraction," The Journal of Supercritical Fluids, 87, pp. 118-128.

[49] Castello, D., Kruse, A., and Fiori, L., 2015, "Low temperature supercritical water gasification of biomass constituents: Glucose/phenol mixtures," Biomass and Bioenergy, 73, pp. 84-94.

[50] Krammer, P., Mittelstädt, S., and Vogel, H., 1999, "Investigating the Synthesis Potential in Supercritical Water," Chemical Engineering & Technology, 22(2), pp. 126-130.

[51] Ondze, F., Boutin, O., Ruiz, J.-C., Ferrasse, J.-H., and Charton, F., 2015, "Supercritical water gasification of beet residues: From batch to continuous reactor," Chemical Engineering Science, 123, pp. 350-358.

[52] Thornton, T. D., and Savage, P. E., 1990, "Phenol oxidation in supercritical water," Symposium on Supercritical Fluids, 3(4), pp. 240-248.

[53] Shen, Z., Yang, D., Wang, S., Wang, W., and Li, Y., 2017, "Experimental and numerical analysis of heat transfer to water at supercritical pressures," International Journal of Heat and Mass Transfer, 108(Part B), pp. 1676-1688.

[54] !!! INVALID CITATION !!! [23, 37, 38].

[55] Aida, T. M., Sato, Y., Watanabe, M., Tajima, K., Nonaka, T., Hattori, H., and Arai, K., 2007, "Dehydration of d-glucose in high temperature water at pressures up to 80 MPa," The Journal of Supercritical Fluids, 40(3), pp. 381-388.

[56] Mokry, S., Pioro, I., Kirillov, P., and Gospodinov, Y., 2010, "Supercritical-water heat transfer in a vertical bare tube," Nuclear Engineering and Design, 240(3), pp. 568-576.

[57] Pioro, I. L., and Duffey, R. B., 2007, "Heat-Transfer Enhancement at Supercritical Pressures," Heat Transfer & Hydraulic Resistance at Supercritical Pressures in Power Engineering Applications, I. L. Pioro, and R. B. Duffey, eds., ASME, New York, NY.

[58] Zhang, R., Zhang, X., and Hu, S., 2015, "Dissolution kinetics of quartz in water at high temperatures across the critical state of water," The Journal of Supercritical Fluids, 100, pp. 58-69.

[59] Killilea, W. R., Swallow, K. C., and Hong, G. T., 1992, "The fate of nitrogen in supercritical-water oxidation," Proceedings of the 2nd International Symposium on Supercritical Fluids, 5(1), pp. 72-78.

[60] Lee, J. H., and Foster, N. R., 1996, "Direct partial oxidation of methane to methanol in supercritical water," The Journal of Supercritical Fluids, 9(2), pp. 99-105.

[61] Portela, J. R., Nebot, E., and Martínez de la Ossa, E., 2001, "Generalized kinetic models for supercritical water oxidation of cutting oil wastes," The Journal of Supercritical Fluids, 21(2), pp. 135-145.

[62] Tiwari, K., Pinkard, B., Gorman, D. J., Davis, J., Kramlich, J. C., Reinhall, P., and Novosselov, I., 2018, "Computational Modeling of Mixing and Gasification in

Continuous-Flow Supercritical Water Reactor," 12th International Symposium on Supercritical FluidsAntibes, France.

[63] Faires, K. B., 2013, "Gasification of in-Forest Biomass Residues," University of Washington.

[64] Behnia, I., Yuan, Z., Charpentier, P., and Xu, C., 2016, "Production of methane and hydrogen via supercritical water gasification of renewable glucose at a relatively low temperature: Effects of metal catalysts and supports," Fuel Processing Technology, 143, pp. 27-34.

[65] Aida, T. M., Shiraishi, N., Kubo, M., Watanabe, M., and Smith Jr, R. L., 2010, "Reaction kinetics of d-xylose in sub- and supercritical water," The Journal of Supercritical Fluids, 55(1), pp. 208-216.

[66] Hendry, D., Venkitasamy, C., Wilkinson, N., and Jacoby, W., 2011, "Exploration of the effect of process variables on the production of high-value fuel gas from glucose via supercritical water gasification," Bioresource Technology, 102(3), pp. 3480-3487.

[67] Vogel, F., Blanchard, J. L. D., Marrone, P. A., Rice, S. F., Webley, P. A., Peters, W. A., Smith, K. A., and Tester, J. W., 2005, "Critical review of kinetic data for the oxidation of methanol in supercritical water," The Journal of Supercritical Fluids, 34(3), pp. 249-286.

[68] Ramayya, S. V., and Antal, M. J., 1989, "Evaluation of systematic error incurred in the plug flow idealization of tubular flow reactor data," Energy & Fuels, 3(1), pp. 105-108.

[69] Ebukuro, T., Takami, A., Oshima, Y., and Koda, S., 1999, "Raman spectroscopic studies on hydrogen bonding in methanol and methanol/water mixtures under high temperature and pressure," The Journal of Supercritical Fluids, 15(1), pp. 73-78.

[70] Sugimoto, K., Fujiwara, H., and Koda, S., 2004, "Raman spectroscopic study on the local structure around O2 in supercritical water," The Journal of Supercritical Fluids, 32(1), pp. 293-302.

[71] Chen, Y., Jin, Z., and Pan, Z., 2012, "In situ Raman spectroscopic study of hydrolysis of carbon tetrachloride in hot compressed water in a fused silica capillary reactor," The Journal of Supercritical Fluids, 72, pp. 22-27.

[72] Jin, J., Wang, J., Shen, Y., Lin, C., Pan, Z., and Chou, I. M., 2014, "Visual and Raman spectroscopic observations of hot compressed water oxidation of guaiacol in fused silica capillary reactors," The Journal of Supercritical Fluids, 95, pp. 546-552.

[73] Braeuer, A. S., 2018, "Prospects: Facing current challenges in high pressure high temperature process engineering with in situ Raman measurements," The Journal of Supercritical Fluids, 134, pp. 80-87.

[74] Aida, T. M., Tajima, K., Watanabe, M., Saito, Y., Kuroda, K., Nonaka, T., Hattori, H., Smith Jr, R. L., and Arai, K., 2007, "Reactions of d-fructose in water at temperatures up to 400 °C and pressures up to 100 MPa," The Journal of Supercritical Fluids, 42(1), pp. 110-119.

[75] Chad, A. L., and Anita, M.-J., 2003, "Automated Method for Subtraction of Fluorescence from Biological Raman Spectra," Applied Spectroscopy, 57(11), pp. 1363-1367.

[76] Zhang, Z.-M., Chen, S., Liang, Y.-Z., Liu, Z.-X., Zhang, Q.-M., Ding, L.-X., Ye, F., and Zhou, H., 2010, "An intelligent background-correction algorithm for highly fluorescent samples in Raman spectroscopy," Journal of Raman Spectroscopy, 41(6), pp. 659-669.

APPENDIX A: PRIMARY COMPONENT LIST AND DOCUMENTATION

- Mixing Section Heater Controller
  - Extech Instruments 48VFL PID Controller
  - http://www.extech.com/resources/48VFL_96VFL_UM.pdf
  - Type K thermocouple
  - 5 Amp relay @ 110V AC
- Primary Heaters
  - HTS Amptek BT15-B2-K-2
  - https://cdn.shopify.com/s/files/1/0283/5140/files/BT15_LIM_Brochure.pdf?1757430451321884 2006
  - Type K thermocouple
  - 15A max current
  - 240V supply
  - BBA-200 Controller
- Reactor Heater Controller
  - Watlow Series C On-Off Temperature Controller
  - https://www.watlow.com/-/media/documents/user-manuals/series-c-rev-e-2-12-08.ashx
  - Switching hysteresis: 1.7°C
  - 120/240V AC, 250VA rating
  - Mechanical switch
  - Type K thermocouple
- Back Pressure Regulator
  - Equilibar U6L1SNN8-NSBP4000T150K30LLK
  - https://www.equilibar.com/PDF/Equilibar-Research_Series-Back_Pressure_Regulators.pdf
  - 1/8” NPT Female Connections
  - Max Pressure: 6000 psi
  - Max Temperature: 150°C
- Reagent Pump
  - SSI Teledyne LS005SFT1C
  - https://ssihplc.com/product-category/hplc-pumps/ls-class/
  - Single piston with prime/purge valve
  - 5 mL/min max flow rate
  - 6000 psi max pressure
  - Leak sensor, pulse dampener, and pressure sensor
  - Micro USB, RS-232, and analog controls
- Water Pump
  - SSI Teledyne LD036SFT1C
  - https://ssihplc.com/product-category/hplc-pumps/ld-class/
  - Double piston with prime/purge valve
  - 36 mL/min max flow rate
  - 6000 psi max pressure
  - Leak sensor, pulse dampener, and pressure sensor
  - Micro USB, RS-232, and analog controls

- Tertiary Pump
    - SSI Teledyne LS005SFT1A
    - https://ssihplc.com/product-category/hplc-pumps/ls-class/
    - 1/16” outlet tubing, otherwise identical to reagent pump
- Raman Cell
    - MarqMetrix MM Raman AIO
    - SN: AIO-M72-2010
    - Sapphire lens
    - 60 ft-lbs torque spec
    - LF4 connections
    - Copper gasket
- Primary Heater (Resistive Coil Heater)
    - Tempco MIGHTY-BAND WITH T/C
    - https://www.tempco.com/Products/Electric-Heaters-and-Elements/Coil-and-Cable-Heaters/Mightyband-Coil-Heaters.htm
    - 0.153” round cable, Alloy 600
    - 0.750” ID x 12” length
    - Type K thermocouple embedded
    - T/C wire length 48”
    - Ungrounded T/C
    - Type S3 termination
    - Sleeve length 46”
    - Type LO1 lead orientation
    - 2000W, 240V
    - 48” of lead wire
- Primary Heater (Ceramic Furnace Heater)
    - OMEGALUX CRFC-412/240-A
    - https://www.omega.com/pptst/CRFC.html
    - 1800W, 240V
    - 12” length
    - Max temperature: 982°C
    - 7” OD, 4” ID
- Mixing Section Heater
    - HTS Amptek AWH-051-020D
    - https://heatingtapes.com/collections/laboratory-tapes/products/duo_tape_hi
    - 0.5” x 2’
    - 156W, 120V
    - Max temp: 760°C
- Reactor Heater
    - OMEGALUX CRFC-36/115-A
    - https://www.omega.com/pptst/CRFC.html
    - 700W, 120V
    - 6” length
    - Max temperature: 982°C
    - 5” OD, 3” ID
- Primary Heat Exchanger

    - Graham Manufacturing 8SP-10 Heliflow Heat Exchanger with Inconel-625 tubes and manifolds, cast steel shell side, and Durlon 8500 casing gaskets and Klinger/C-4401 manifold gaskets
    - http://www.graham-mfg.com/usr/Brochures/heliflow.pdf
    - Max pressure 5500 psi
    - Max temperature 650°C
    - 1492W heat rejection at 1.0 gpm flowrate
- Closed Loop Heat Exchanger
    - Lytron MCS50G02BC1
    - http://www.lytron.com/Cooling-Systems/Standard/Ambient-Cooling-Systems?tab=specs
    - 3500W cooling capacity
    - ½" NPT Female connections
    - 55°C Maximum liquid temperature
    - 120V, 5.8A
    - 1.8 gpm flowrate
- Tubing
    - High Pressure Medium Pressure and Taper Seal fittings (LF & AF connections)
    - 1/16" & 1/8" tubing is 316SS, ¼" is a mix of Inconel 625 and 316SS, ¾" tubing is Inconel 625
    - Translucent plastic tubing is PTFE or PFA
    - Rubber hoses are Neoprene with zinc-plated steel fittings, ¼" NPT
- Coiled Reactor Section
    - Inconel 625
    - LM4 Medium Pressure Connections
    - 72" total length (182.88 cm)
- Thermocouples
    - Omega 1/16" Type K Thermocouple with Alloy 600 sheath